Thesis for The Degree of Licentiate of Engineering

Platinum-Based Nanocatalysts for Proton Exchange Membrane Fuel Cells

Björn Lönn

Department of Physics
Chalmers University of Technology
Gothenburg, Sweden, 2023

Platinum-Based Nanocatalysts for Proton Exchange Membrane Fuel Cells

Björn Lönn

Department of Physics
Division of Chemical Physics
Chalmers University of Technology
SE-412 96 Göteborg,
Sweden
Phone: +46(0)31 772 1000

Cover:
Sputtering synthesis of platinum-based nanoparticles in liquid PEG. TEM images show the nanocatalyst before and after attachment to a high surface area carbon support, via heat treatment.

Printed by Chalmers Digitaltryck,
Gothenburg, Sweden 2023.

"Be positive"
- Proton, to the electron

Platinum-Based Nanocatalysts for Proton Exchange Membrane Fuel Cells

Björn Lönn

Department of Physics
Chalmers University of Technology

Abstract

Fuel cells have potential to become an integral technology in a future sustainable energy system. For transport applications, the proton exchange membrane fuel cell (PEMFC) is the most promising option, exhibiting light weight and high energy density. However, large-scale commercialization is impeded by expensive catalyst materials and slow oxygen reduction reaction (ORR) kinetics on the cathode side. Several alternatives to the conventional platinum PEMFC catalyst have been proposed and studied during the last decades, one being platinum-rare earth (Pt-RE) metal alloys. With enhanced ORR activities and maintained stability, these materials are highly interesting for deployment in PEMFCs, and could potentially reduce both catalyst material use and overall fuel cell cost. In practical fuel cells, catalysts are required in nanoparticulate form, to facilitate sufficient performance while keeping material utilization high. Unfortunately, scalability remains as a main obstacle for Pt-RE nanoparticle synthesis, as fabrication of these materials has proven challenging, motivated by the high oxygen affinity of the rare-earth metals.

This thesis investigates the use of sputtering onto liquid (SoL) substrates as a potential synthesis method for Pt-RE nanocatalysts. The influence of sputtering parameters, including substrate type and temperature, as well as gas environment, on the size and morphology of platinum-based nanocatalysts are studied. Transmission electron microscopy of platinum sputtered in four different liquids indicates that the size of the nanoparticles is only weakly dependent on temperature. Furthermore, catalyst layers fabricated from the SoL-synthesized nanocatalysts are evaluated in a half cell setup. The electrochemical results shows that high performing catalyst layer fabrication from SoL-synthesized nanoparticles is viable, which opens for further development of the technique.

Keywords

Fuel cells, Pt-RE nanocatalysts, Sputtering onto liquids

List of Publications

Appended publications

This thesis is based on the following publications:

I **Plasma-Induced Heating Effects on Platinum Nanoparticle Size During Sputter Deposition Synthesis in Polymer and Ionic Liquid Substrates**,
R. Brown, B. Lönn, R. Pfeiffer, H. Frederiksen, B. Wickman
Langmuir 37.29 (2019), 8821-8828.

II **Platinum Nanoparticle Fuel Cell Catalyst Layers Synthesized by Sputtering onto Liquid Substrates**,
B. Lönn, M. Luneau, B. Wickman
In manuscript.

Other publications

The following manuscript has been submitted during my studies but is not included in the thesis.

Stability of ORR activities on a carbon supported Pt3Y thin film in a PEMFC,
E. Marra, G. Montserrat-Sisó, B. Eriksson, B. Lönn, R. Wreland Lindström, G. Lindbergh, B. Wickman, C. Lagergren
Submitted to *Electrochimica Acta*. 2023

My contributions

Paper I

I performed the temperature measurements during sputtering, authored that part of the paper and implemented review comments.

Paper II

I performed all experiments and wrote the manuscript.

Contents

Chapter 1

Introduction

Climate change stands as mankind's most demanding challenge, hitherto. It is well established that the increasing global temperatures observed during the recent century originates from human activities, and in particular, rising levels of greenhouse gas (GHG) emissions of modern society [1]. Detrimental effects are currently reported on land [2] as well as in the oceans and the cryosphere [3]. To mitigate these effects, and to reduce the risks of escalating climate issues, preventive actions are of utmost importance. Around the globe, work is conducted by individual governments [4] and larger, inter-governmental organizations [5, 6] to facilitate a transition towards a fossil-free energy system. The 2015 United Nations Climate Change Conference (COP 21), held in Paris, saw the implementation of the latest global UN treaty on climate change. Subsequently called the Paris Agreement, the treaty was signed by 196 parties, with a primary goal to limit "the increase in the global average temperature to well below 2°C above pre-industrial levels" [7]. However, several reports show that the National Determined Contributions of the countries within the Paris Agreement, are far from meeting the emission targets necessary to limit global temperature rise to 2°C [8, 9], which underlines the importance of large scale collaborations and initiatives to reduce the temperature increase.

The recent commitment of the European Union [5] to become "The first climate-neutral continent" by 2050, in an effort titled European Green Deal, marks an important step towards net-zero GHG emissions. Part of this exertion, is shifting from a fossil based energy system, to one relying on renewable energy sources, mainly wind and solar. A transition of this type, being unequivocally needed, does however, not come without challenges. One of the major challenges for green energy based on solar and wind power, is its intermittency and the associated gap between electricity supply and demand. This factor, alongside with the ongoing increase in global electricity usage, embodies the need for higher degrees of electricity security during the transition into clean energy [10]. One potential approach to improve energy grid balance, is to use hydrogen as energy carrier. In an energy system relying to large extent on variable renewable electricity sources, probable scenarios could see hydrogen being produced via the process of electrolysis, utilizing excess renewable electricity to split water

into its elements, hydrogen and oxygen. Hydrogen produced in this way has several uses: as base chemical for the chemical industry, reducing agent in the production of fossil-free steel, fuel in transportation applications, or as temporary energy storage to stabilize the electricity grid on a later occasion. In fact, the system presently described, commonly denoted as a Hydrogen Economy, constitutes an important part of the European Green Deal [11].

Fuel cells are the most efficient technology for back-conversion of hydrogen to electricity. The process utilizes the chemical reaction between hydrogen and oxygen, forming only water as product, to convert the chemical energy back to electricity. Compared to conventional combustion, fuel cells offer several advantages, including higher efficiencies and, if hydrogen is produced from renewable energy, zero emissions, crucial to a future sustainable energy system.

1.1 Thesis scope

Fuel cells come in many variants and their different inherent advantages makes them suitable for a wide range of applications. This thesis concern the development and evaluation of catalyst materials for proton exchange membrane fuel cells (PEMFCs), the most widespread fuel cell technology for transport applications. So far, large-scale commercialization of PEMFCs, has been hindered by their high cost, mainly as a consequence of using noble platinum as catalyst material to ensure satisfactory performance and durability. As will be argued in chapter 4, there exist a need for new PEMFC catalyst materials, but traditional synthesis techniques are unsuitable for one of the most promising catalyst candidates, the platinum rare-earth (Pt-RE) metal alloys. The aim of this thesis is to give new insights into how the relatively young technique of sputtering onto liquids (SoL) could unlock the full potential of Pt-RE alloys. To reach there, gaining knowledge about fundamental processes involved in the catalyst synthesis, how it relates to basic catalyst properties including size and morphology, and its link to catalytic activity and fuel cell performance, is essential and indeed the overarching goal of this thesis.

The upcoming three chapters will introduce the concepts of catalysis, electrochemistry and PEMFCs. Chapter 5 contains descriptions of the methods and experimental techniques used throughout the work related to the thesis. In chapter 6, I will present some of the results from this work, parts of which are included in papers I and II, while chapter 7 summarizes the conclusions and insights drawn, and gives an outlook for future work.

Chapter 2

Catalysis

Catalysis, the act of accelerating the rate of a chemical reaction via addition of a non-consumable substance (catalyst), has been used by humanity since the dawn of civilization, exemplified by the fermentation of sugars into alcohol in ancient times [12]. The participation of a substance, not consumed by the overall reaction, to enable combustion, was reported already in 1794 by Elizabeth Fulhame [13, 14]. It was, however, not until the early-to-mid 19^{th} century that the term catalysis appeared [15], and a solid theory started to be built around its characteristics. Today, the importance of catalysis to modern society cannot be overstated. To give a few important examples, catalysts are widely used in the chemical industry for production of pharmaceuticals, fertilizers, base chemicals and petroleum products [16, 17]. In addition, during the last 50 years, catalysts are an indispensable part of emission control in fossil fueled vehicles [18]. Unsurprisingly, catalysts are important also for fuel cell applications.

The main field of catalysis can be be subdivided into two branches, homogeneous and heterogeneous catalysis. What separates the two concepts from each other, is the relationship between the phases in which the catalyst itself, and the reactants are present. In homogeneous catalysis, the catalyst is in the same phase as the reactants, typically in liquid phase. On the contrary, in heterogeneous catalysis the catalyst is in a different phase than the reactants. Commonly, a solid phase catalyst is used to increase the rate of liquid or gas phase reactions. Heterogeneous catalysis is used in hydrogen fuel cells, which utilizes solid phase catalysts and gas phase reactants.

2.1 Heterogeneous catalysis

The reaction rate of a catalytic reaction is determined by the interactions occurring between reactants and the catalyst surface. To understand the reaction rate, it is necessary to mention the concept of activation energy. According to the Arrhenius equation (2.1) [19], the rate constant of a reaction k, is related to the temperature T by an exponential expression containing the activation energy of the reaction E_a, the gas constant R and a pre-exponential

factor A.

$$k = Ae^{\frac{-E_a}{RT}} \tag{2.1}$$

The rational behind the Arrhenius activation energy is that in order for a set of reactants to transform into reaction products, an energy barrier (E_a) needs to be overcome. The reaction rate constant can be thought of as the number of collisions between reactants which results in a reaction, during some unit of time. For an uncatalysed reaction in gas or liquid phase, the pre-exponential factor reflects the total amount of collisions between reactants per unit time, and the exponential term the probability of such collisions to result in a reaction. It is evident from equation 2.1 that an increase in temperature or a decrease in activation energy will improve the rate of the reaction. This is intuitive since at higher temperatures, more collisions will take place, and for lower activation energies, a larger percentage of collisions will result in a reaction to occur.

A catalysed reaction provides an alternative reaction pathway, typically involving a series of elementary steps at the catalyst surface: adsorption of reactants, surface diffusion, surface reaction, and desorption of products. Associated with all four steps is, to varying extent, the ascent of energy barriers. Figure 2.1 illustrates how such a catalysed reaction pathway could look, in comparison with the uncatalysed reaction. As depicted in the figure, the

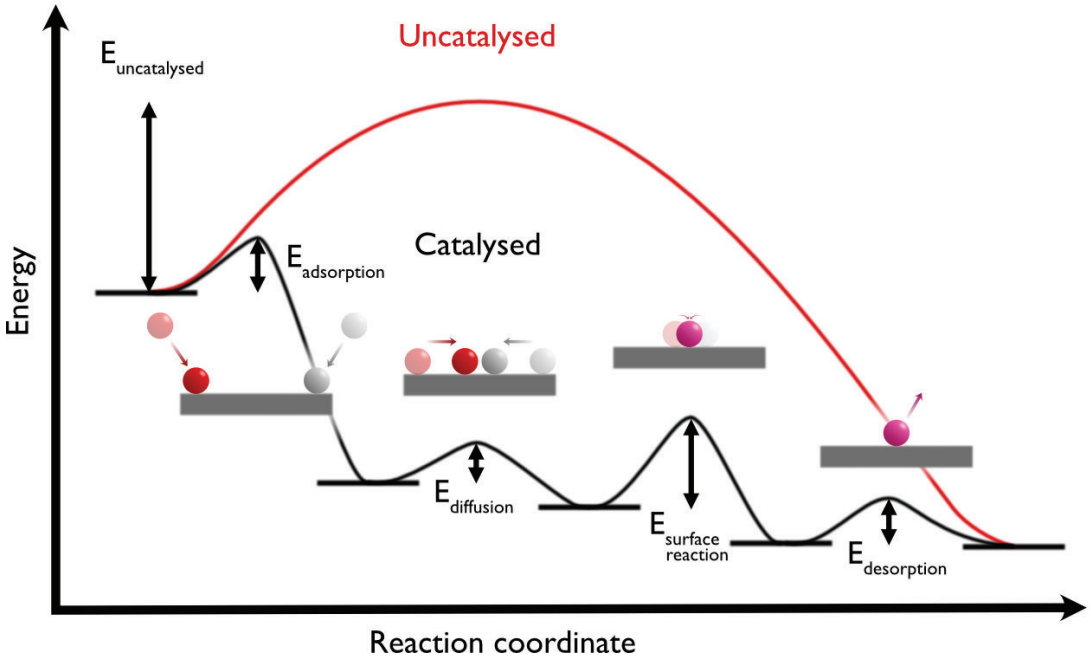

Figure 2.1: Qualitative energy diagram of a chemical reaction showcasing both the catalysed, and the uncatalysed reaction path.

individual elementary steps of the catalysed pathway, all exhibit energy barriers smaller than the uncatalysed reaction, resulting in faster overall reaction rate.

When evaluating the potential of a material to catalyse a specific chemical reaction, it is common to investigate the binding energies of the the different reactants, intermediates and products. For a catalyst to perform well, it is important that its binding strength with any such specie is neither too high

nor too low. If the binding is too weak, reactants and intermediates will either not bind, or desorb before any reaction takes place, while if too strong, efficient blocking of active sites will arise by products or intermediates. The concept of relating binding strength to catalytic activity is called Sabatier's principle [20], and results in a volcano-shaped plot as shown i figure 2.2. The best catalysts for the reacton in question, are found close to the top of the volcano at a corresponding optimum binding energy E_{opt}.

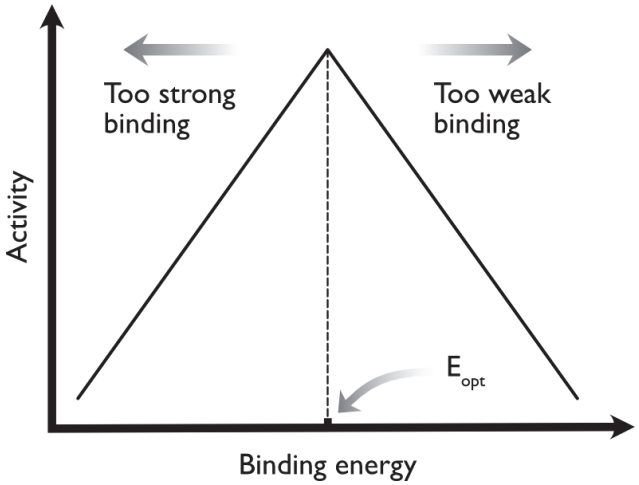

Figure 2.2: Sabatier's principle illustrated in the form of a volcano plot of catalytic activity versus binding energy of an arbitrary specie.

Another important factor to consider in catalyst development, is the catalysts ability to selectively promote the wanted reaction(s), while suppressing the unwanted ones. While a deeper discussion on PEMFC catalysis is left for chapter 4, it is at this stage sufficient to stress the importance of developing cheaper and more efficient PEMFC catalysts. To succeed, the target catalyst should approach the top of the volcano in terms of activity towards the relevant reactions, while exhibiting both good selectivity, promoting water formation over hydrogen peroxide, and long-term stability. Before returning to the topic in 4.5, follows a chapter on the scientific field on which fuel cells rest, namely electrochemistry.

Chapter 3

Electrochemistry

Electrochemistry is a scientific field devoted to the interplay between electric potentials and chemical reactions. This often involves the study of redox reactions and their response under the influence of an electric potential or the passage of a current, but equally interesting are sometimes the opposite process, meaning how a spontaneous reaction can be utilized to convert chemical energy into electricity. The latter case is our main concern, when considering energy conversion in fuel cells. The aim of this chapter, is to provide a fundamental base of the concepts of electrochemistry that are most closely related to fuel cells. Starting off with a brief history and explanation of fundamental concepts, following up with a more detailed description of redox reactions and general electrochemical systems, before turning the focus to fuel cells in the next chapter.

3.1 Fundamentals

Although widespread interest in fuel cells and hydrogen economy is a relatively new phenomenon, electrochemistry, as well as basic fuel cell technology, is old. In fact, the history of electrochemistry spans multiple centuries of scientific discoveries [21, 22], from electricity-induced twitching of frogs legs and the first electric battery in the late 1700's, to alkaline fuel cells in space during the 1960's and the cutting-edge research in fuel cells, electrolyzers and batteries of modern days. I will not delve much further into the general history of electrochemistry, but rather offer an expanded discussion on the implications of its fundamental concepts, before narrowing down to detailed descriptions of the same concepts.

The fact that electric potentials and currents are interlinked with a group of chemical reactions, called redox reactions, has large implications when observed through the lenses of thermodynamics [19]. According to thermodynamics, reactions can be either spontaneous, meaning that they occur naturally by themselves, while releasing some amount of energy to its surroundings, or non-spontaneous, requiring input of energy from the surrounding. If a certain redox reaction occurs spontaneously, parts of its released energy will become

accessible, in the form of electrons or, more specifically, an electric current. This is often utilized in so called galvanic cells. What is also implied, is that by providing a certain amount of energy which can be done by application of an electric potential, a redox reaction can be forced to run in its non-spontaneous direction. A system based on this idea, is denoted as an electrolytic cell. Some of our fundamental and most important energy technologies, including batteries, fuel cells and electrolyzers, all operate according to these premises, which will now be discussed in further detail.

3.2 Redox reactions

To understand electrochemical systems, a central concept is redox reactions, a certain class of chemical reactions in which electrons are transferred between two species, causing a change in oxidation states of the species. The name stems from reduction-oxidation, which is most easily explained as the two opposite processes of gaining and loosing electrons, respectively. As a simple example of a redox reaction one can consider the expression given in equation 3.1

$$X + Y \rightarrow X^{n+} + Y^{n-} \tag{3.1}$$

where transfer of n electrons occur between the chemical species X and Y. Here, n+ and n- denotes electron loss and gain, respectively. X is being oxidised into X^{n+} and Y is reduced to form Y^{n-}. Species that accepts electrons to become reduced (Y), are called oxidants (Ox), while electron donors (X) are denoted as reductants (Red). This allows us to identify two types of pairs in equation 3.1, namely the *redox pair* X/Y and the two *redox couples* X/X^{n+} and Y^{n-}/Y, where each redox couple consists of a reducing specie (X or Y^{n-}) alongside its oxidising form (X^{n+} or Y). The overall redox reaction above can be treated as two separate *half reactions*, one for the oxidation (3.2) and another for the reduction (3.3). When considering half reactions, it is advisable to include the transferred electrons as a term in the expression, according to equations 3.2 and 3.3.

$$X \rightarrow X^{n+} + ne^- \tag{3.2}$$

$$Y + ne^- \rightarrow Y^{n-} \tag{3.3}$$

The two processes of oxidation and reduction always occur in pairs and simultaneously, however they may be separated in space, a fact that is extensively utilized in various electrochemical systems.

3.3 Electrochemical systems

An electrochemical system typically consists of two or more electrodes, separated in space and connected via both an electric circuit and an ionic conducting

media or electrolyte, see figure 3.1. Electrodes facilitate the half reactions by either collecting electrons released by the oxidation reaction (anode), or supplying electrons to the reduction reaction (cathode). As a result, a flow of electrons will occur in the external electric circuit, from the anode to the cathode. Similarly, ions generated at one of the electrodes, will flow through the ion conducting media separating the two electrodes. Here, the direction of ionic flow depends on the type of cell and more specifically on the choice of electrolyte. Positive ions will move towards the cathode, while negative ions move in the direction of the anode.

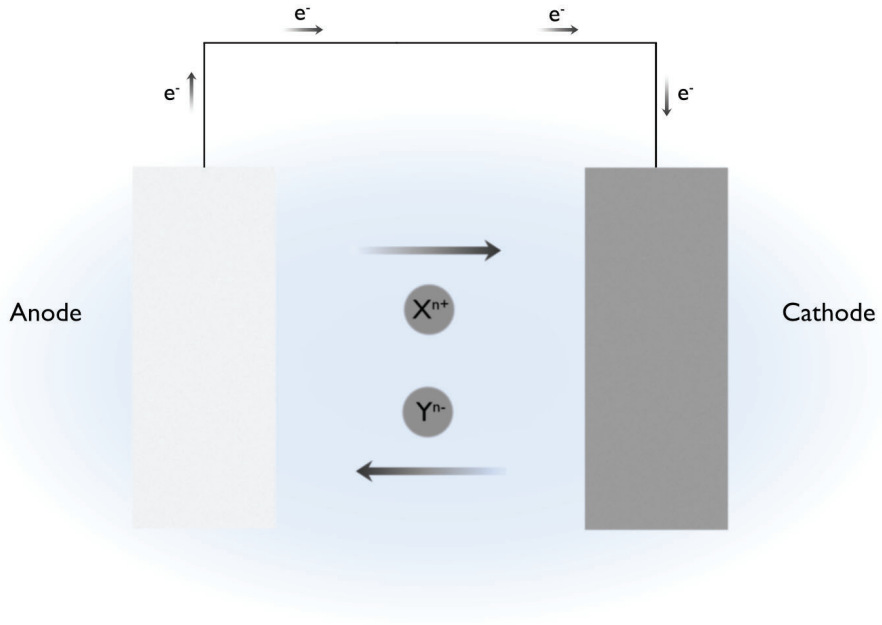

Figure 3.1: General schematic of an electrochemical cell containing two electrodes, a cathode and an anode.

3.3.1 Electrode potentials and cell potential

Connected to each electrode is an electrode potential ($E_{cathode}$ and E_{anode}), corresponding to the reduction potential of its related half reaction [19, 23]. The reduction potential is a measure of how easily the oxidising agent of the redox couple is reduced, and corresponds to the potentials at which the half reaction produces no net current, meaning that the forward and backward reaction rates are at equilibrium. Its value is given relative to that of a reference potential, typically that of the hydrogen electrode reaction at standard conditions, which is referred to as 0 V.

$$\frac{1}{2}H_2 \rightleftharpoons H^+ + e^- \tag{3.4}$$

When a redox reaction takes place in an electrochemical cell, the total potential of the cell will be the difference between its respective electrode potentials.

$$E_{Cell} = E_{cathode} - E_{anode} \tag{3.5}$$

This cell potential E_{Cell}, gives the theoretical maximum amount of work W_{max} that can be obtained from a redox reaction involving the transfer of n electrons, through

$$W_{max} = -nFE_{Cell} \tag{3.6}$$

where the Faraday constant F (96 485 C/mol), correspond to the electric charge of one mole of electrons. W_{max} is also the minimum amount of work that needs to be applied in order to force the reactions of 3.1-3.3 to occur in the opposite direction.

3.3.2 Thermodynamics

Redox reactions are, just as all other chemical reactions, governed by the laws of thermodynamics. Considering a redox reaction in its most general form,

$$Ox + ne^- \rightleftharpoons Red \tag{3.7}$$

consisting of a reduction process in the forward direction (cathodic) and an oxidation in the backward direction (anodic), with n electrons being transferred. Gibbs free energy of the reaction ΔG is related to that under standard conditions ΔG^0, via

$$\Delta G = \Delta G^0 + RTlnQ_r \tag{3.8}$$

T being temperature, R the gas constant and $Q_r = \frac{a_{Red}}{a_{Ox}}$ the reaction quotient or the relative amount of products and reactants. ΔG is known as the maximum work accessible from a chemical reaction. Combining equations 3.6 and 3.8 gives

$$E_{Cell} = -\frac{\Delta G}{nF} = -\frac{\Delta G^0}{nF} - \frac{RTlnQ_r}{nF} = E^0_{Cell} - \frac{RTlnQ_r}{nF} \tag{3.9}$$

which is known as the Nernst equation, relating the cell potential to its equilibrium potential at standard conditions when no net current flows through the electrodes.

3.3.3 Overpotential

When an electrochemical system is used for the conversion of chemical energy into electricity (galvanic cell), or vice versa (electrolytic cell), the conversion efficiency will always be less than 1 [23, 24]. The explanation lies in the fact that every real system is affiliated with losses, throughout the system. For a galvanic cell, the maximum power output depend on the cell potential, at each specific current. Due to the different system losses, there will be a difference between the actual cell potential of the cell E_{Cell}, and the theoretical value derived from the reduction potentials of the participating electrode reactions E_0. Hence, the

cell potential, and therefor also the power output, is reduced as a result of the losses in a galvanic cell, as illustrated in figure 3.2. Conversely, for electrolytic cells, more input power is required to maintain the reactions, resulting in an increase in cell potential from its reversible value. The difference between

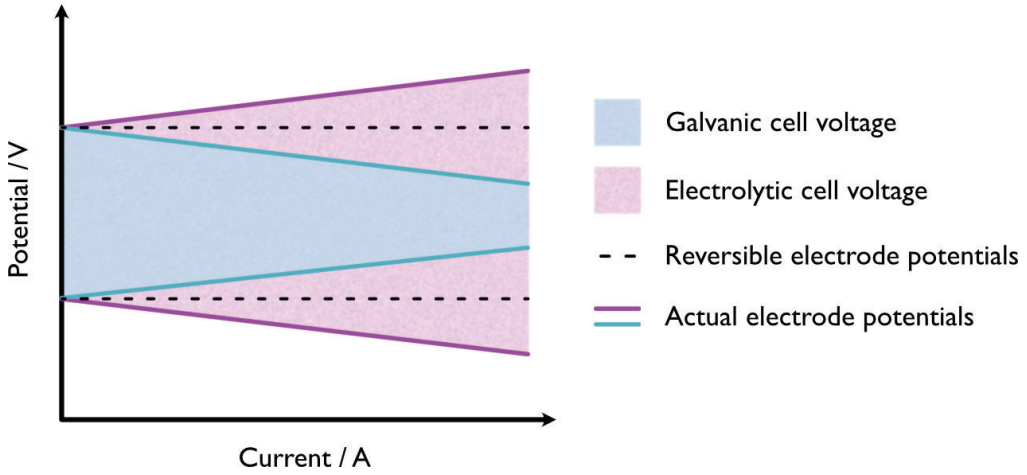

Figure 3.2: Simplified illustration of current-voltage dependence of galvanic (turquoise) and electrolytic (pink) cells. Electrode potentials are indicated by solid lines, while equilibrium potentials are shown as dashed lines Coloured areas between the solid lines display how the respective cell voltage of galvanic and electrolytic cells change with increasing currents.

the cell potentials and the reversible potential in electrochemical systems is known as *overpotential*, $\eta = \mathrm{E}_{Cell} - \mathrm{E}_0$. Similarly, the overpotential at specific electrodes can be defined as the difference between its observed potential to the reversible, equilibrium potential.

In reality, this current-voltage dependence is not linear as in figure 3.2, and for proper modelling, all types of losses needs to be accounted for. At low to moderate currents, where most losses can be attributed to reaction barriers, the electrode potentials of most electrochemical systems can be described by the Butler-Volmer equation [25], relating the current to electrode overpotential by

$$i = i_0 \left(e^{\frac{(1-\alpha)nF\eta}{RT}} - e^{\frac{-\alpha nF\eta}{RT}} \right) \tag{3.10}$$

where i_0 is the so called exchange current at equilibrium and α a charge transfer coefficient, describing how efficiently electrons are supplied from the electrode to the reaction. At higher currents, other types of losses starts to play a role as will be discussed in 4.4, and equation 3.10 needs to be adjusted for such effects.

3.3.4 Applications

Electrochemical principles are the basis for several fundamental energy technologies, including batteries, fuel cells and electrolysers. A fuel cell converts chemical energy stored in a fuel, to electricity according to the mechanisms described for a galvanic cell above. Electrolysers are instead electrolytic cells,

in which electrical energy is supplied to drive a chemical reaction. In this way, hydrogen can be produced for subsequent deployment using a fuel cell. Batteries are, similarly to fuel cells and electrolysers, energy converters. The big difference between batteries and fuel cells, is that batteries act directly as energy storage, while fuel cells require external storage and continuous supply of fuel to produce electricity. Furthermore, rechargeable batteries acts as electrolytic cells while charging and galvanic cells during discharge. In general, batteries offer exceptional energy conversion efficiencies, outperforming both fuel cells and electrolysers in this regard. However, batteries suffer from low gravimetric energy density, making them heavy and not well suited for heavy-duty and long-range transport. Fuel cells offer both lighter weights and faster refuelling, compared to batteries, making them an attractive alternative for these types of applications.

Chapter 4

Proton Exchange Membrane Fuel Cells

Fuel cell history is almost as old as that of electrochemistry. Credited with the invention of the first fuel cell in 1838, is William Robert Grove [21, 26, 27], following his work on a fuel cell incorporating alternating sheet iron, copper and porcelain plates, immersed in a copper sulphate - diluted acid solution. Later, in the early 1930's, Francis Thomas Bacon started developing the first practical, alkaline fuel cell, and his technology was later proven useful in the Apollo space missions [21, 22]. Fuel cell technology has developed tremendously since its early days, and today exists many different types of fuel cells. The proton exchange membrane fuel cell (PEMFC) is the most widespread type due to its large range of applications [28], particularly within the transport sector. It is also the technology to which the focus of this thesis will be addressed. Before going further into the details of PEMFCs and their fundamental theory, a brief review of other important fuel cell technologies, and the advantages of PEMFCs, will follow.

4.1 Other fuel cell types

Fuel cells come in many different designs, all of which have their specific, inherent advantages and disadvantages. Furthermore, what aspects and traits that are most crucial is most often application dependent. One way to categorize fuel cells is to group them by their operating temperature, leading to the identification of two main classes: low temperature- and high temperature fuel cells. High temperature fuel cells are mainly aimed for stationary applications [28] where better utilization of their high heat output is possible and the need for start-stop situations are few. Two examples of high temperature fuel cell chemistries are solid oxide and molten carbonate. As their names suggest, the electrolytes in these types of cells consist of either a solid oxide, often a mix of zirconia and yttria, or a molten carbonate, typically sodium and potassium carbonate, supported by a ceramic matrix [28]. The reactions of these types of

fuel cells are facilitated at elevated temperatures in the range of 600-1000 °C and utilizes a wider range of fuels than the low temperature systems.

Low temperature fuel cells on the other hand, are typically operated below 100 °C and employ a variety of different chemistries. A clear distinction is that between PEMFCs and anion exchange membrane fuel cells (AEMFCs), based on acidic and alkaline electrolyte membranes, respectively. These types of fuel cells are, much due to their low operating temperatures, highly suited for applications within mobility and other areas where high power output per weight is important [28, 29].

Regardless of the type and chemistry, all fuel cells share the same overall function and components, although nomenclature sometimes differ.

4.1.1 Advantages of PEMFCs

The fact that PEMFCs operate at low temperatures is accompanied by several advantages compared to its high temperature relatives. At high temperatures, both thermal and mechanical properties of fuel cell components become increasingly important. Hence, PEMFCs offer lighter weights and more flexibility in material selection and modularity [28]. Another advantage is the fast start-up times which, together with its high energy density makes PEMFCs the most widely considered fuel cell technology for transport applications, where weight and start-up time are some of the most important aspects [28, 29]. When compared to other low temperature fuel cells, such as the AEMFC, one main advantage is the lower sensitivity to CO_2-poisoning, which readily reduces the performance and durability of AEMFCs [30, 31]. Additionally, PEMFCs exhibit better ionic conductivity, due to the faster transport of H^+ ions compared to OH^- for AEMFCs.

4.2 Components

The general components of a PEMFC are its two electrodes (cathode and anode) and a proton exchange membrane (PEM). To the electrodes belong an assembly of carbon supported catalyst layers, gas diffusion layers (GDLs) and flow field plates for transport of reactants and products, current collectors and a frame for stability. An overall schematic of a single cell is shown in figure 4.1. Many single cells are generally stacked in series to to form a fuel cell stack and boost the power output. Then reactant and product transport, current collection and mechanical stability are all provided by one single component called a bipolar plate. Although fuel cell stacks are the most relevant configuration for real applications, I will limit this discussion to the components of a single cell PEMFC.

Proton exchange membrane

The heart of a PEMFC and the origin of its name, is the proton conducting membrane, specifically constructed to allow transport of protons from the anode to the cathode, while acting as an impermeable barrier for electrons,

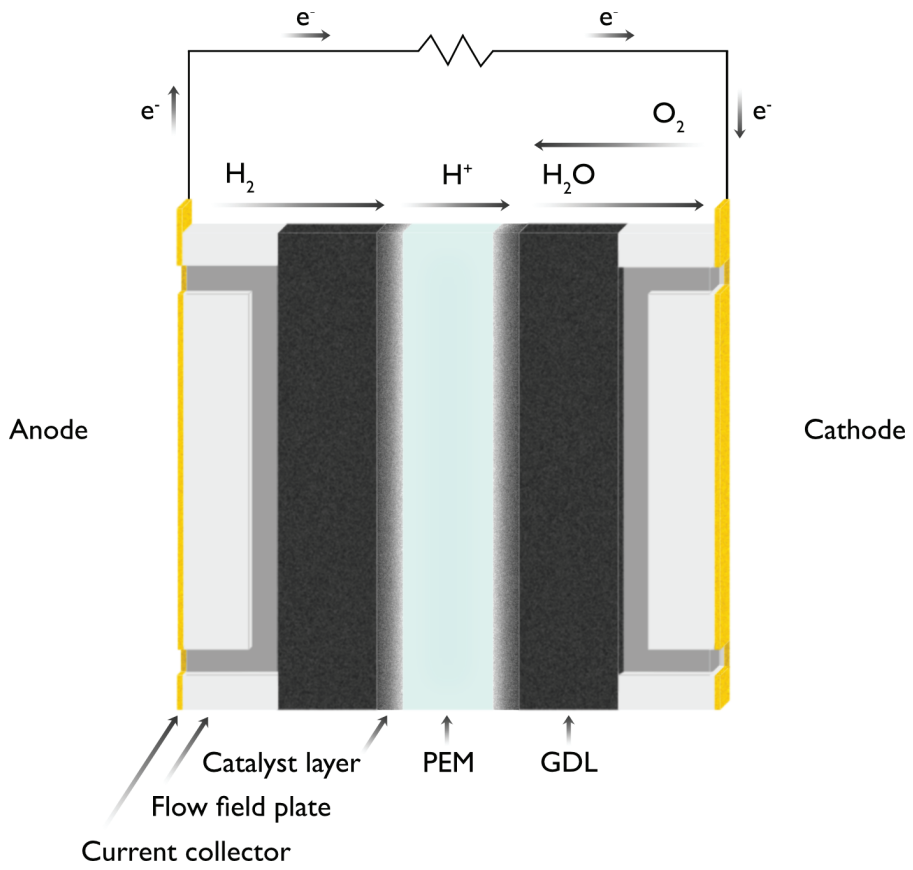

Figure 4.1: PEMFC schematic, showcasing the different components and directions of electron, ion, reactant and product flows indicated.

reactant gases and the reaction product, water [32]. The most common PEM types are different kinds of perflourosulfonic acids, consisting of perflourinated polymer backbones with sulfonic acid functionalized sidechains grafted onto the backbone. The perflourinated backbone gives the membrane its mechanical strength and prevents excess swelling when exposed to water, while the hydrofilic sulfonic acid groups allows absorption of water, which is necessary for ion conduction through the membrane [33]. Proton conduction in these types of membranes occur via two distinct mechanisms, diffusion induced by the potential difference between the cathode and anode, and the Grotthuss mechanism in which proton hopping takes place between the absorbed water molecules in the membrane. The diffusion mechanism is considered to contribute the most to the overall proton conductivity of perflourinated sulfonic acid membranes [34].

Electrodes

Both the anode and cathode side of a PEMFC consists of a catalyst layer, GDL, flow field and a current collector. Furthest away from the membrane are the current collector and the flow field, whose respective task is to provide the transport of either electrons or reactants and products, to and from the electrode-membrane interfaces. Flow fields are typically a metal plate with

incorporated channels to simplify the flow of gases and water. Between the flow field and the catalyst layer sits the GDL, typically a fibrous carbon paper or cloth [24]. Its purpose is to provide an even distribution of reactant gases and electric current to the catalyst layer, efficiently remove the water produced in the reaction and add mechanical stability for the catalyst layer [24, 35].

The most common catalyst layer configuration is that of platinum nanoparticles supported on a highly porous, large surface area carbon structure as depicted in figure 4.2. Being the closest layer to the PEM, high porosity and surface area are important to ensure good contact with protons in the membrane, and allow transport of reactants to the catalyst surface. In addition, the carbon supported catalyst layer needs to provide good electric contact, for removal or supply of electrons to the respective electrode reactions.

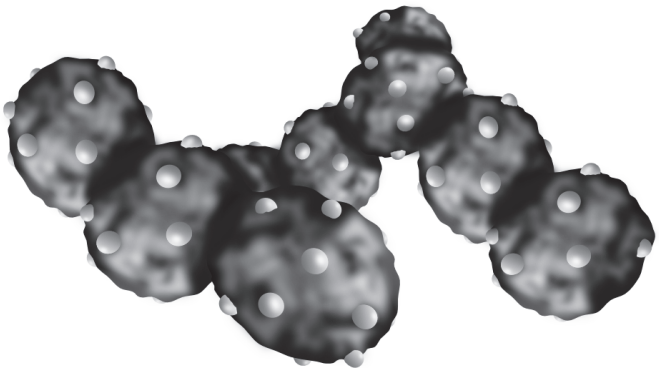

Figure 4.2: Platinum catalyst nanoparticles (white) supported on a porous structure of high surface area carbon (black).

4.3 Reactions

The overall reaction of a PEMFC is that of hydrogen and oxygen reacting to form water as the sole product.

$$2H_2 + O_2 \rightarrow 2H_2O \tag{4.1}$$

The reaction can, in similarity to all other redox reactions, be described by its two half reactions, oxygen reduction and hydrogen oxidation. The half reactions are inherent to all types of hydrogen fuel cells, although their stoichiometries differs depending on the medium. The reaction pathways described here are those valid in acidic media.

4.3.1 Hydrogen oxidation reaction

At the anode side of a PEMFC, hydrogen is oxidised by the dissociative splitting of hydrogen molecules into protons and electrons, in a half reaction denoted as the hydrogen oxidation reaction (HOR).

$$H_2 \rightarrow 2H^+ + 2e^- \tag{4.2}$$

The reaction is of simple nature as it involves only two elementary steps, and is readily catalysed by platinum with only small losses.

4.3.2 Oxygen reduction reaction

The oxygen reduction reaction (ORR) is the cathode side half reaction in a PEMFC. In acidic media, ORR consists of the combination between oxygen, protons and electrons,

$$O_2 + 4H^+ + 4e^- \rightarrow 2H_2O \tag{4.3}$$

to form water. This is called the four electron pathway as it involves four electrons for every oxygen molecule being reduced. A competing reaction pathway exists, in which an oxygen molecule combines with two electrons and two protons,

$$O_2 + 2H^+ + 2e^- \rightarrow H_2O_2 \tag{4.4}$$

forming hydrogen peroxide. For fuel cell applications however, this two electron pathway is unfavorable, since it results in less current.

The reduction potential of the ORR half reaction is +1.23 V at ambient conditions. Recalling that the reduction potential of the anode half reaction, HOR, is defined as 0 V, the theoretical maximum cell potential of a PEMFC at ambient temperature and pressure, is 1.23 V. As we will see, the current-voltage behavior of PEMFCs are far from the ideal case. Comparing expression 4.2 and 4.3 of HOR and ORR respectively, it is evident from the amount of participating reactants, and therefor the number of elementary steps required, that the complexity of ORR considerably exceeds that of HOR. This makes the cathode reaction of PEMFCs rate limiting, and constitutes one of the major sources of losses in this type of systems.

4.4 Losses

The concept of overpotential was introduced in chapter 3, and it is now time to discuss the different types of losses that give rise to the cell potential drop in operating fuel cells. Generally, three types of losses can be described, namely *activation losses* in the electrode, *ohmic losses* in the membrane, electrodes and external circuitry, and losses due to inefficient *mass transport* of reactants and products [24].

Activation losses

Recalling the concept of activation energy introduced in chapter 2, chemical reactions involve the overcoming of an energy barrier, in order for the reaction to take place. Catalysts are used to decrease these barriers and speed up the reactions, however, a certain energy barrier will always remain, and its amplitude is highly reaction dependent. In a PEMFC, the energy required to drive the HOR and ORR half reactions will result in an instant drop of the cell

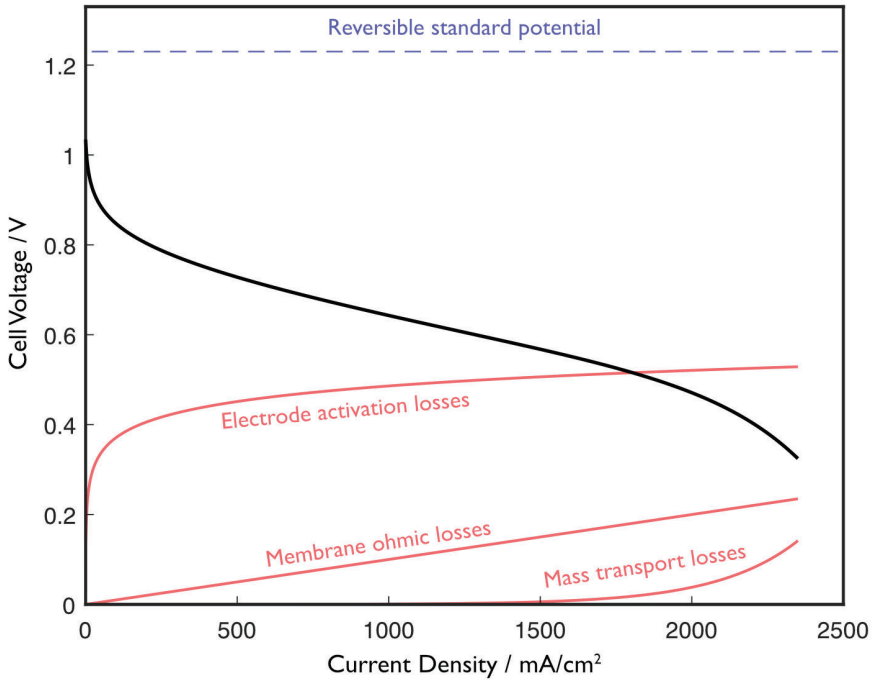

Figure 4.3: Qualitative illustration of a PEMFC performance curve (black), with approximate activation, ohmic and mass transport losses indicated (red).

potential, at zero current according to figure 4.3. As we start to draw current from the PEMCF, a highly non-linear voltage dependence can be observed in the current, while for larger currents, the activation losses becomes more linear in nature. The largest part of the activation losses originate from the ORR on the cathode side.

Ohmic losses

Any electric or ionic conductor is associated with a certain amount of resistance towards the flow of electrons and ions, respectively. In a PEMFC, resistive losses occur both in the electrolyte membrane, the electrode materials and various electric interconnections. The response, in the form of a cell potential drop, is approximately linear with increasing currents. Hence, as reflected in figure 4.3, its impact is small for low currents but becomes a concern in higher power situations.

Mass transport losses

As the current in a fuel cell increases, so does the consumption of reactants at the electrodes. According to the Nernst equation (3.9), reactant concentrations affect the electrode potentials. Therefore, inefficient supply of fresh reactants to the electrodes decreases the overall cell potential of the cell. At a PEMFC cathode, where oxygen is supplied in the form of air, inert nitrogen, not consumed by the reaction, can effectively block the transport of fresh oxygen to the electrode, at high currents [24]. Further blocking can arise if the reaction

product, water in the case of PEMFCs, is not removed at an adequate rate. Mass transport losses are responsible for the voltage breakdown at high currents indicated in figure 4.3, and as a consequence, these high current regions are normally avoided in fuel cell operation.

4.5 Catalyst Materials

The PEMFC is, due to its acidic nature along with fluctuating operating potentials, a very harsh environment for catalyst particles. As a result, noble platinum is the most widely used PEMFC catalyst material, exhibiting both good chemical stability and high catalytic activity towards the HOR and ORR reactions. However, platinum is scarce and expensive, which is an obstacle for large-scale commercialization of PEMFCs. To facilitate a widespread transition of heavy-duty, long range transport into a fuel cell-based sector, platinum utilization must become better.

Alternatives

When discussing alternative replacements for platinum in PEMFCs, as well as catalyst materials for any application in general, there are three main aspects to consider:

- Activity
- Stability
- Selectivity

The catalytic activity, meaning the catalysts ability to accelerate a certain reaction, is naturally of high importance when designing new catalysts. The better the catalytic activity, the lesser material is needed to obtain satisfactory performance. However, unless the catalyst is also stable in the electrochemical environment of the PEMFC, a high initial activity is relatively ineffective. Finally, selectivity is important to ensure that only the desired reaction occur. In PEMFCs, as mentioned in 4.3.2, a competing reaction to the main four-electron cathode side reaction is the two-electron pathway, which results in less current as only half the number of electrons are involved in this type of ORR. Hence, a good PEMFC catalyst material should promote the four-electron ORR pathway.

One way to improve the ORR activity of a catalyst is to alter its binding energy to oxygen species, which can be done by alloying. For platinum, which is already close to the top of the volcano plot of figure 4.4, a weakening of the oxygen binding energy of roughly 0.1 eV is needed to reach the optimum. The two main groups of platinum alloying agents that has been reported for ORR are the late transition metals, with cobolt and nickel being the most studied [36–40], and the rare-earth metals, including yttrium [41–48] and the lanthanides [42, 49–51].

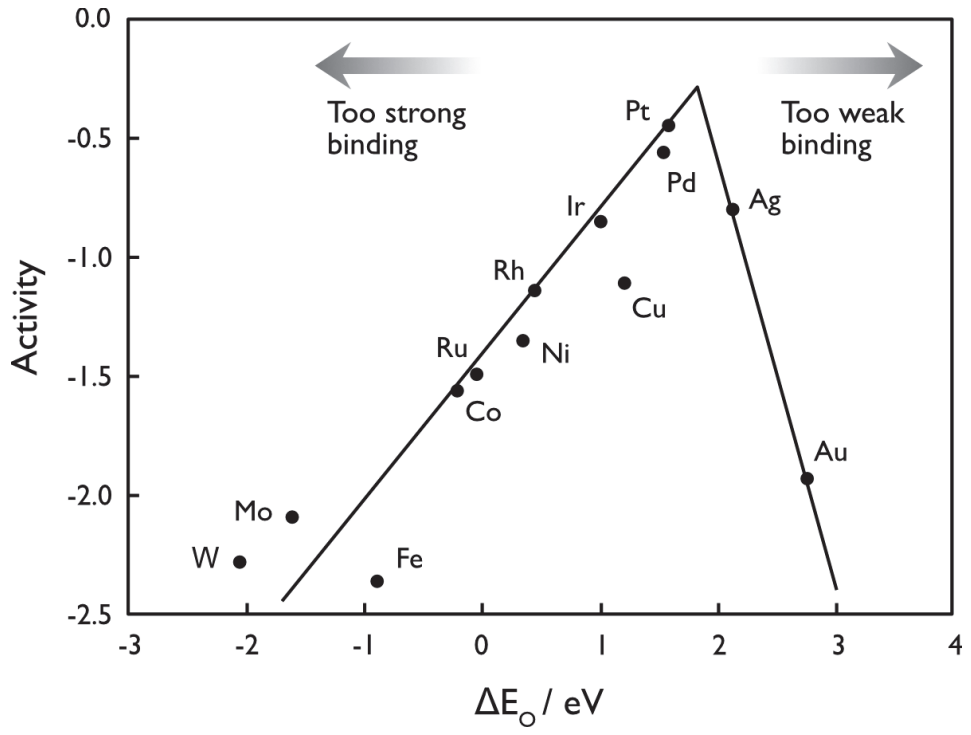

Figure 4.4: Volcano plot for the ORR activity as a function of O binding energy. Data is from [52].

Platinum-late transition metal alloys have the advantage of exceptional ORR activities, reaching enhancement factors of up to 10 times that of polycrystalline platinum [36], but they suffer from dealloying during long-term operation [53, 54]. Platinum-rare earth metal (Pt-RE) alloy activity enhancements have been reported as comparable to those of platinum-late transition metal alloys. In addition, they exhibit more favorable alloy formation energies, resulting in better catalyst stability [43]. The reason for both their enhanced activities and stabilities, is the formation of a thin, pure platinum skin at the material surface [51], when exposed to acidic environment. The platinum overlayer, about a nm thick, is affected by the lattice mismatch with the alloy core underneath, which induces a compressive strain in the shell [50]. This strain has been attributed to cause a slight weakening of the binding energy with oxygen species, and hence to increase the specific ORR activity [41].

For Pt-RE nanoparticles, the amplitude of the strain, and its associated specific ORR activity enhancement has been shown to increase with nanoparticle size [41]. When increasing the size of a particle, the surface to volume ratio decreases inversely proportional to the radius. Consequently, to ensure high catalyst material utilization, the activity per unit mass is an important parameter for nanoparticle catalysts. Since for Pt-RE alloys, there is a trade-off between specific activity and surface to volume ratio, there exists a specific particle size at which a maximum in the mass activity is reached. By mass-selection of sputtered nanoparticles, the optimal nanoparticle sizes for Pt_xY [41] and Pt_xGd [49] has been shown to be in the range of 8-10 nm. This can be put into perspective when compared to the optimum of 3 nm, for pure

platinum particles [55].

While various techniques have been used to display the excellent ORR activities of Pt-RE nanoparticles, no technique has yet been able to provide scalability while maintaining the ultra-high catalytic performance in terms of activity and stability. The extreme reduction potentials and oxygen affinities of the rare earth elements effectively prevents the use of conventional nanoparticle synthesis routes. A gap exists within the collection of synthesis techniques, to both meet the high requirements of the rare earth metals, and enable fabrication of high performance fuel cell catalyst layers. If Pt-RE alloys are to become a competitor to platinum as standard PEMFC catalyst, this gap needs to be addressed.

Chapter 5

Methods and Experimental Techniques

To fill the Pt-RE nanoparticle synthesis gap mentioned in previous sections, this thesis investigates a technique based on magnetron sputtering onto liquid substrates, in an attempt to address both the low oxygen partial pressure requirement, and the issue of catalyst layer fabrication. This chapter gives a brief background of the techniques used for the work performed. Largest focus is paid to central concepts for nanocatalyst synthesis and electrochemical characterization.

5.1 Nanocatalyst synthesis

5.1.1 Magnetron sputtering

Principle

Sputtering is a physical vapor deposition (PVD) technique utilizing the impact energy of an ionized sputter gas, such as argon or krypton, to knock out atoms and clusters of a target material. This is done through the application of a voltage across the gas, eventually forcing it to ionize, forming a plasma glow. Without the addition of any further restricting equipment, this plasma will simply fill the space between the negatively biased sputter target (cathode) and the positively biased substrate (anode). The positively charged ions, are attracted by the cathode, forcing an acceleration towards the target plate. Upon impact, depending on the applied voltage, one or more atoms and atomic clusters may be ejected from the surface as a result of the collision. The principle, called sputtering, was interestingly enough discovered in 1852, [56] by the same W.R. Grove also credited for the invention of the fuel cell.

In magnetron sputtering, an arrangement of magnets behind the target plate, typically one central magnet surrounded by a ring of magnets of opposite polarity, give rise to a magnetic field. Depending on the strengths of the individual magnets, two different configurations of the magnetic field may arise,

as depicted in figure 5.1. If the strength of the centre magnet is as high as its surrounding magnets, all field lines exiting the outer magnets will pass through the middle magnet. Such a configuration is called a balanced magnetron, and leads to confinement of the plasma close to the target plate, as its electrons are trapped by the magnetic field lines, and disallowed to ionize gas molecules in the rest of the chamber.

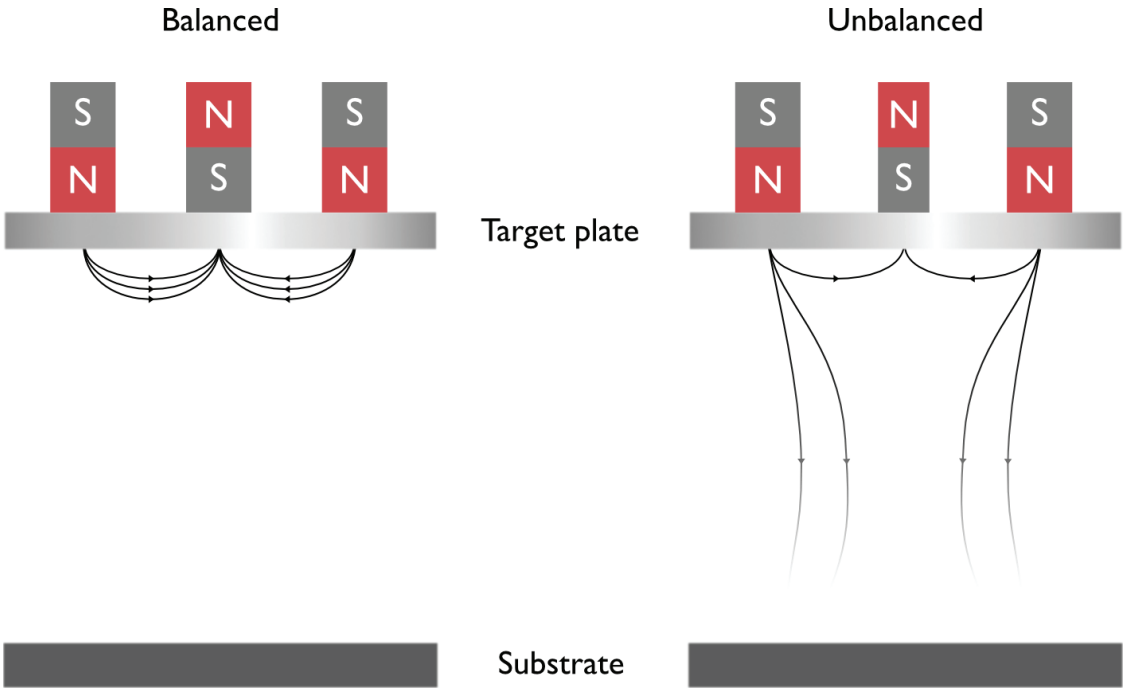

Figure 5.1: Schematic of the two different magnetron configurations, balanced and unbalanced.

If instead the center magnet is weaker than its surrounding counterparts, it will not be able to close all field lines. As a result, electrons will escape the confinement, ionize neutral gas molecules further away from the target, and hence, allowing the protrusion of plasma onto the substrate. This type of configuration is called an unbalanced magnetron and is the type that has been used in this thesis.

Liquid substrates

The magnetron sputtering technique is widely used for thin films within micro- and nanofabrication, but its application is not limited to various types of layered structures and coatings. Pioneering work in the mid 1990's [57] on using low vapor pressure liquids as substrates for sputtering, quickly developed into a new, facile and multi-purposed method for nanoparticle synthesis. The advantages of sputtering onto liquids (SoL) are several, including long term stabilization of nanoparticles provided by the liquid, the lack of capping agents needed as well as the use of a pure target plate over chemical precursors, which are often difficult to remove and sometimes hazardous.

The practice of SoL generally consists of the insertion of a low vapor pressure liquid supported on a glass wafer, or inside an open container, to a vacuum

chamber. The liquid substrate is mounted underneath the magnetron gun with the target plate, at some target-to-substrate distance. Low vapor pressure liquids are required to withstand the ultra-high vacuum (UHV) conditions inherent to the magnetron sputter chamber. Evacuation to base pressures of less than $5 \cdot 10^{-7}$ mbar, is obtained by turbomolecular pumping. UHV conditions are especially important when considering synthesis of Pt-RE alloy nanoparticles, to prevent oxidation of the rare-earth metal. A simplified schematic of the SoL procedure is shown in figure 5.2, illustrating the plasma shape resulting from an unbalanced magnetron configuration. During sputtering, the protruding plasma causes the liquid substrate to heat up. Heating the substrate ultimately decreases its viscosity and increases the diffusion rate of immersed particles, clusters and single atoms, which can be used to tailor the size of nanoparticles [58] by controlling the temperature. Sputtered atoms and clusters are ejected in a complicated emission pattern, depending on ion energies and incident angles as well as target texture [59]. Here, it is sufficient to understand that a portion of the ejected atoms and clusters will propagate through the target-to-substrate gap, and impinge on the liquid surface. Due to collisions between, and subsequent coalescence of atoms and clusters within the sputter gas, the population of sputtered species arriving at the substrate surface will be a mix of atoms, clusters and nanoparticles.

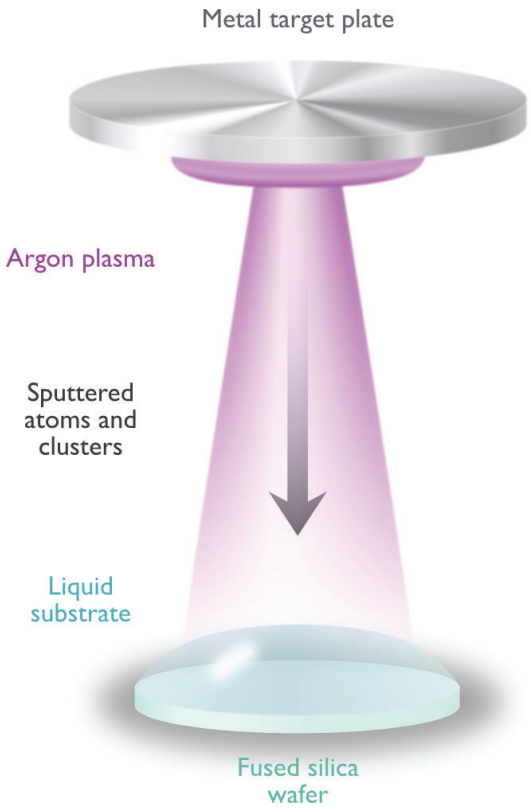

Figure 5.2: Schematic illustrating the SoL technique.

Further nucleation, growth and sometimes aggregation may occur inside the liquid. Except for viscosity, nanoparticle growth and aggregation is also governed by the interactions between the substrate and submerged particles.

The interaction is highly dependant on the type of substrate. Two noteable examples are those of ionic liquids and polymers. An ionic liquid consists of an ion pair, a positively charged cation, and a negative anion. These ions can, depending on the charge of the submerged nanoparticles, arrange themselves in an electric double layer around the particles. Polymers, on the other hand, are long chains of hydrocarbons, that can surround the nanoparticles and provide steric stabilization. The exact amount of stabilization provided by both groups of substrates, depends on the specific choice of liquid. To summarize the applicability of liquid substrates in nanoparticle synthesis, a correctly chosen liquid will act both as a combined collection and growth medium, and provide the stabilization needed for aggregation prevention.

5.1.2 Attachment of nanocatalyst particles on carbon support material

For real applications inside fuel cells, immobilization of nanocatalyst particles onto a high surface area carbon support material and addition of an ionomer, is required to facilitate reliable electrical and ionic contact, as well as transport of reactants and products. Common carbon support materials are various types of Vulcan® and Ketjenblack®, while the most common ionomer is Nafion®. It is essential to find a route for catalyst particle transfer from the liquid substrates, and attachment to the carbon support.

One method for nanoparticle transfer and attachment has been used in this thesis, and consists of a heat treatment of the liquid stabilized nanoparticles, along with Vulcan® XC-72. The support material is simply ground and added to the nanoparticle-liquid substrate dispersion, after which the mixture is heated to 150 °C in an oil bath for 19 hours, under constant magnetic stirring. After the heat treatment, a supported catalyst powder was extracted by repeated washing in isopropanol and separation by centrifugation, followed by a drying step in an oven at 80 °C overnight.

5.2 Physical characterization

Physical characterization is used to investigate important properties of the SoL-synthesized nanoparticles, including size and morphology as well as chemical states and composition.

5.2.1 Transmission electron microscopy

The resolution limit of an optical microscope, commonly known as the Abbe limit of diffraction [60], states that the minimum resolvable distance d is directly proportional to the wavelength of transmitted light λ by

$$d = \frac{\lambda}{2NA} \tag{5.1}$$

where NA is the numerical aperture of the objective lens. Assuming a wavelength in the shorter region of visible light (400 nm), and a numerical

aperture around 1.5, typical for modern optical microscopes, the minimum distance that can be resolved becomes 133 nm. Considering the typical size of practical fuel cell catalyst nanoparticles is in the range of 3-10 nm, another imaging technique is required to obtain high enough spatial resolution. As a consequence of the wave-particle duality, electrons can be used for imaging in a similar manner as light. With wavelengths considerably shorter than light, electron microscopy offers supreme spatial resolution compared to its optical counterpart, in the order of Ångströms [60].

In transmission electron microscopy (TEM), thin specimens (up to 100 nm) are subjected to a high energy electron beam. Due to the high energy of the incident beam, electrons will, to large extent be transmitted or forward scattered by the sample, allowing their use for imaging in an analogous manner to traditional optical microscopes.

5.2.2 Small-angle X-ray scattering

Small-angle X-ray scattering (SAXS) is a technique for characterization of small objects, such as nanoparticles or polymers, using a collimated X-ray beam [61]. When the beam hits the sample, it interacts with the atoms of the particles, and any scattering or absorption events is thence reflected in the resulting output signal. The scattering pattern obtained, is an average of all the particles within the sample, hit by the beam. By looking at the scattered signal at small detection angles, information about the average size and shape of nanoparticles in the sample can be retrieved, which is particularly useful when concerned with structure and morphology of nano-objects.

5.2.3 X-ray photoelectron spectroscopy

While SAXS utilizes scattering of X-rays directly, X-ray photelectron spectroscopy (XPS) is based on an indirect effect of X-ray interactions with the sample [62]. When an X-ray beam hits the sample, interactions with atoms of the sample will cause it to scatter within a relatively large volume of the material. At some point, the photons will be absorbed by an atom, donating its energy to one of the atoms electrons. If the absorbed energy is larger than the combination of its binding energy and the work function of the system, the electron will be emitted from the atom. Such an electron is denoted a photoelectron. For known energies of incident photons, the kinetic energy of the ejected photoelectron will be directly related to the binding energy of the electron, which is an element specific characteristic. As a consequence, detection of photoelectrons offers a way to determine the chemical states as well as composition of materials. Additionally, while the mean free path of X-rays are typically large in most materials, mean free paths of photoelectrons are not [62]. This means that only photoelectrons from the absolute top surface layer will escape into the vacuum and reach the detector, making XPS a surface sensitive technique.

5.3 Electrochemical characterization

Electrochemical characterization allows evaluation of the catalytic performance of synthesized catalysts, which can be subsequently linked to the physical properties. This section discuss the electrochemical methods used in this thesis.

5.3.1 Cell setup

In this work, all electrochemical characterization was performed using a rotating disk electrode (RDE) setup, including a potentiostat, a rotator and an electrolyte-filled three-electrode glass cell. The operating principles of the potentiostat is left out of this thesis, however, it can be understood as an instrument for controlling and measuring potentials and currents. The three electrodes of the glass cell are denoted as working (WE), counter (CE) and reference (RE) electrodes, respectively. As WE in the measurements conducted here, a certain type of electrodes called glassy carbon electrodes (GCE) is used, with the purpose of constituting a simple platform for electrochemical evaluation of electrocatalysts. The GCE geometry chosen was that of small cylinders, typical for RDE, which can be coated by deposition of a catalyst thin film or as in this work, by a layer of catalyst nanoparticles on microporous carbon, which will be described in 5.3.2. The coated WE is mounted at the end of a Teflon head connected to a rotatable shaft according to figure 5.3. The WE provides the location for the half reaction of interest, while the other half reaction is facilitated at the CE. Upon application of a potential over the two electrodes, a resulting current will start to flow in the external connection between them, which can be measured by an amperemeter in the potentiostat. As electrons are either added or removed at the WE, the CE needs to perform the opposite action in order to balance the overall charge of the system. In doing so, the CE voltage will vary considerably and it is therefor not viable to directly measure the voltage between the WE and CE. Instead, the exact potential of the WE is measured relative to the RE, in which a well-defined redox reaction equilibrium fixes its potential at a stable, known value. This technique is not affected by the reactions on the other two electrodes, as no current passes through the RE.

5.3.2 Electrode preparation

The most common process for preparation of nanocatalyst layers on GCEs is via drop casting of a catalyst ink. The ink is typically made by dispersion of the supported catalyst powder in a solvent, by ultrasonication. A Nafion solution is added to the ink, acting both as a glue and ion conductor in the final electrode. Catalyst ink is drop casted onto small (5 mm in diameter), cylindrical GCEs under slow rotation, to provide more homogeneous coverage of the electrode surface, and heating from a heat gun facilitates faster drying of the catalyst layer. No material is lost in this process, meaning that catalyst loading can be derived directly from the concentration in the ink.

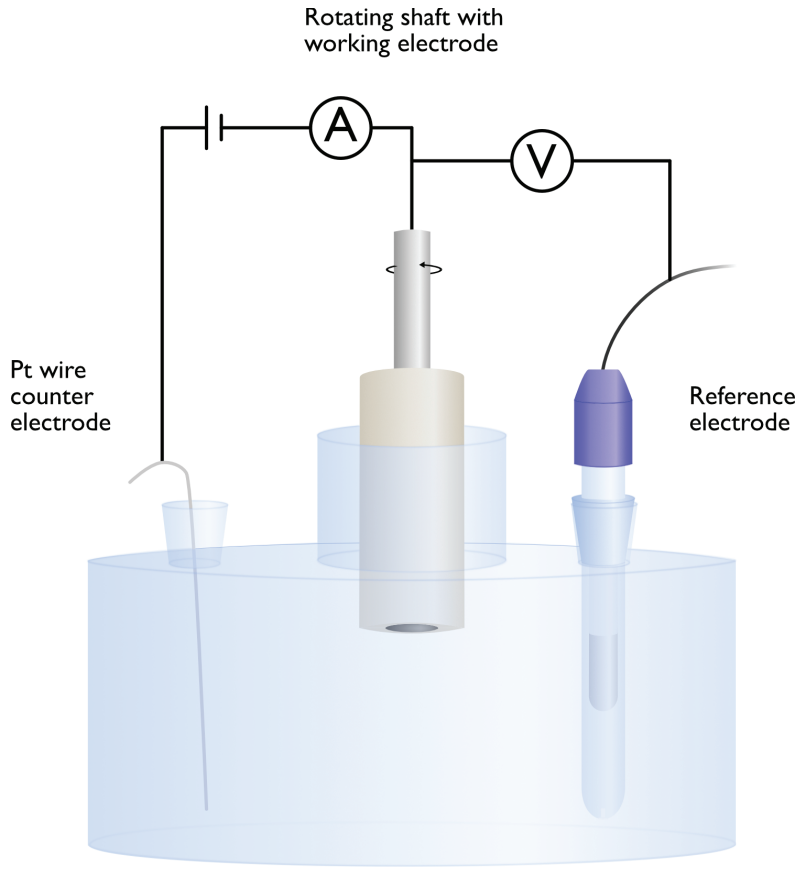

Figure 5.3: Combined three-electrode RDE cell setup employing a platinum wire CE, catalyst-coated glassy carbon WE and an RE.

5.3.3 Cyclic voltammetry

Cyclic voltammetry (CV) is a technique used to characterize the nature of redox reactions [23], by measuring the resulting currents while continuously sweeping the potential between two limiting values, upon which currents are often plotted as a function of the potential. When a platinum WE is cycled between 0.05 and 1 V, in an electrolyte saturated with inert gas, typically nitrogen or argon, the voltammogram will exhibit a current-voltage behaviour governed by the adsorption and desorption of oxygen and hydrogen species from the electrolyte, onto the catalyst surface. The CV curve of figure 5.4 illustrates the redox behaviour of hydrogen and oxygen species on platinum nanoparticles in argon saturated 0.1 M perchloric acid ($HClO_4$) electrolyte, cycled between 0.05 and 1.0 V at 50 mV/s scanrate. In the CV, positive currents are denoted as anodic, meaning that the WE acts as anode, with a flow of electrons from the electrolyte to the electrode, as species are being oxidized. Similarly, negative currents (cathodic) represents the reduction of electrolytic species, demanding the transfer of electrons from the electrode into the electrolyte. Here, the WE acts as cathode. Looking at the curve of figure 5.4, three main potential regions can be identified, displaying distinct features, these being below 0.4 V, 0.4-0.6 V, and above 0.6 V. At lower potentials, a set of distinct peaks are observed. These belong to what is usually called under-potential deposition

(UPD), or adsorption and desorption of hydrogen. As we move towards higher potentials in the plot, a flat region of comparably low currents appear, the so called double layer region. Here, there are no active redox reactions, and all currents belong to the charging of an electrolytic double layer at the electrode surface. This capacitance layer is not unique to the double layer region, but is always present when sweeping or cycling the potential. Above 0.6 V, another set of peaks develop, which originate from the adsorption/desorption of oxide species and the oxidation of platinum. Two important features, not visible in the CV of figure 5.4, is the evolution of hydrogen (HER) and oxygen (OER), respectively. HER would be reached by sweeping the potential slightly further in the cathodic direction, passing 0 V, while oxygen evolution typically requires potentials of closer to 1.6 V, where the onset potential for OER on platinum is located.

The adsorption and desorption of oxygen and hydrogen species from the electrolyte, and the charging of the electric double layer capacitance, is an artefact of the potential cycling. This means that as soon as the potential cycling is stopped, there will be no currents produced from these processes. Continuous electrochemical reactions on the other hand, are not dependent on potentials being swept or cycled to produce current. Currents produced in this manner, are called Faradaic currents, while currents from the other processes are denoted as non-Faradaic currents.. An example of a continuous electrochemical reaction is when the electrolyte is bubbled with oxygen, for which ORR takes place for potentials below 1 V. It is worth noting that in a CV, the contribution of non-Faradaic currents will always be added as an overlay to the Faradaic currents.

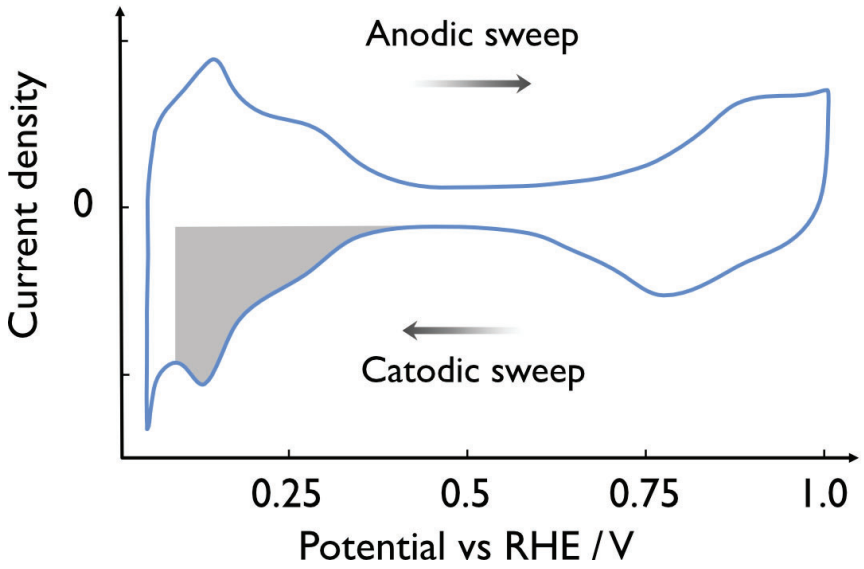

Figure 5.4: Typical CV of platinum nanoparticles in argon saturated 0.1 M $HClO_4$, indicating the directions of anodic and cathodic sweeps, as well as the hydrogen UPD integral area used for ECSA calculations.

5.3.4 Evaluation of electrochemical surface area

There are many techniques for electrochemical surface area (ECSA) measurements in acidic medium [63]. For measurements on platinum fuel cell catalysts, underpotential deposition (UPD) of hydrogen and CO-stripping are two commonly used methods. The first can be performed directly using the argon CV of figure 5.4. The currents involved in either the adsorption (marked in grey), or desorption (not marked) of hydrogen on the catalyst surface, can be related to the total charge of hydride film formation via

$$Q = \frac{1}{\nu} \int IdE \tag{5.2}$$

where ν is the scan rate. It is important to stress that only the contribution from hydrogen adsorption is used, and the double layer capacitance current is therefore subtracted beforehand. Typically, the integration is made from the double layer region, to the local maxima right before hydrogen evolution starts (figure 5.4). The charge obtained from integration over this range, is generally considered to corresponds to a hydrogen coverage of 77% [64]. On obtaining the charge from the hydrogen layer, it can be compared to the theoretical value of hydrogen monolayer formation on the specific catalyst. For hydrogen on platinum, this charge θ_{Pt} is assumed to correspond to one electron per platinum site, giving a monolayer charge of $\theta_{H-Pt} = 210$ μC cm_{Pt}^{-2} [64]. Hence, an estimation of the ECSA is attained from:

$$A_{ECSA} = \frac{Q}{0.77 \cdot \theta_{H-Pt}} \tag{5.3}$$

A second approach to estimate the ECSA is by the process of CO-stripping. The idea is analogous to that of hydrogen UPD, but instead of hydrogen, the catalyst surface is poisoned by carbon monoxide (CO). Then, the electrolyte is purged of excess CO by extensive bubbling with inert argon. After argon purging, only a monolayer of CO is left on the surface, upon which a standard CV is initiated. Adsorbed CO will become oxidized into CO_2 and desorb from the surface, from which a CO-stripping current peak is formed somewhere within the 0.5-0.9 V potential range. Via subtraction of the following CV, and subsequent integration, the charge related to the CO oxidation is obtained in the same manner as for the hydrogen UPD. Then, the ECSA is again estimated by the monolayer charge. As CO oxidation involves the transfer of two electrons, the monolayer charge will be twice that of hydrogen UPD, $\theta_{CO-Pt} = 420$ μC cm_{Pt}^{-2}, giving the ECSA as:

$$A_{ECSA} = \frac{Q}{\theta_{CO-Pt}} \tag{5.4}$$

5.3.5 Rotating disk electrode

In a fuel cell, with pressurized gases continuously supplied to the electrodes, mass transport losses arise first when attempting to draw rather high currents. In a three electrode cell however, the system will experience mass transport

losses also at low currents, caused by the low reactant concentrations in the electrolyte, and the presence of a stagnant layer at the electrode surface (figure 5.5), through which reactants need to diffuse for any reaction to occur. This becomes a problem when characterizing the kinetic performance of the catalyst, at low overpotentials. By using an electrode mounted to a rotating shaft, an RDE setup, the issue can be mitigated. The rotational motion of the shaft (figure 5.5) will induce an electrolyte flow towards the electrode, which in the immediate vicinity of the electrode surface, becomes laminar in its radial direction. The stagnant diffusion layer will become thinner, as the rotation rate increases, and mass transport losses due to slow diffusion hence become decreasingly influential.

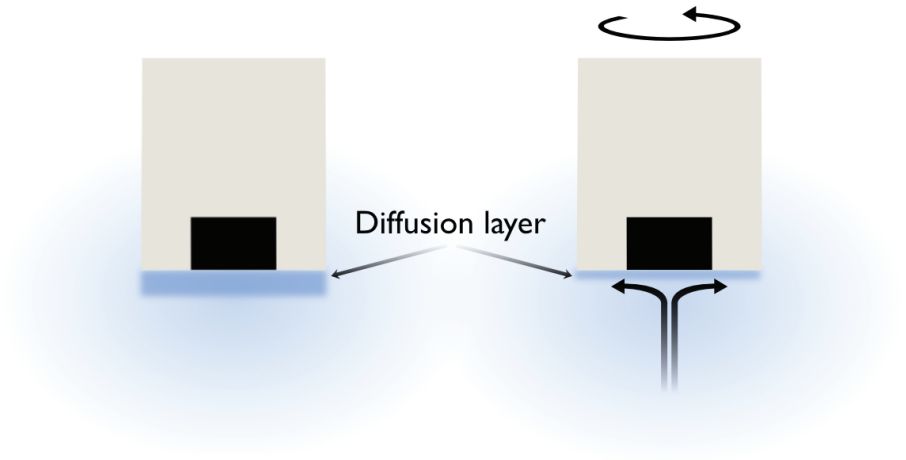

Figure 5.5: Cross-section of the RDE shaft and GCE, with diffusion layers and electrolyte flow indicated for the two cases of no rotation (left), and with rotation (right).

A main concern of this thesis, is the study of oxygen reduction on potential fuel cell cathode catalysts. The catalytic ORR performance is evaluated in RDE, by saturating the electrolyte with oxygen, cycling the potential between 0.05-1.0 V and recording the resulting current, all while rotating at 1600 rpm.

Chapter 6

Platinum-Based Nanocatalysts Sputtered onto Liquid Substrates

As discussed in chapter 4, the particle size of Pt-RE nanoparticles affect the ORR activity. As we are investigating a new technique (SoL) for synthesis of these materials, it is important to obtain an understanding of the fundamental mechanisms behind nanoparticle nucleation and growth in SoL. In an effort to do so, we started to investigate the behaviour of platinum, as it is a more widely studied material, allowing for better comparison with literature. Recently, we applied the technique on the Pt_3Y alloy.

This chapter will summarize and discuss the key points of **papers I** and **II**, with a special focus on the parts to which I made significant contributions, as well as other results, obtained throughout the work, that was not included in any of the mentioned papers.

6.1 Influence of synthesis parameters

The many different parameters which may influence nanoparticle nucleation and growth in SoL can be categorized into three main groups: Those of the substrate (viscosity, surface tension, liquid type etc.), the sputter gas environment (pressure, sputter gas species etc.) and magnetron gun parameters (voltage, sputtering power etc.). Here, I will mainly discuss the influence of liquid substrate type and temperature, as well as gas environment, on the nanoparticle nucleation and growth processes. However, it should be mentioned that our unbalanced magnetron setup is utilized for controlled substrate heating, by applying a range of sputtering powers. Hence, the size effect seen from heating the substrate in this work, is a combined effect,

consisting of contributions from both altering the sputter power, and the associated substrate heating.

6.1.1 Liquid substrate

In **paper I**, four different low-temperature liquids were used as sputtering substrates, three imidazolium-based ionic liquids (Emim Tf, Dmim Tf and Dmim Tf_2N), and the polymer, PEG 600. Nanoparticle size was studied using both TEM and SAXS, and the resulting mean diameters are shown in figure 6.1, with standard deviations indicated.

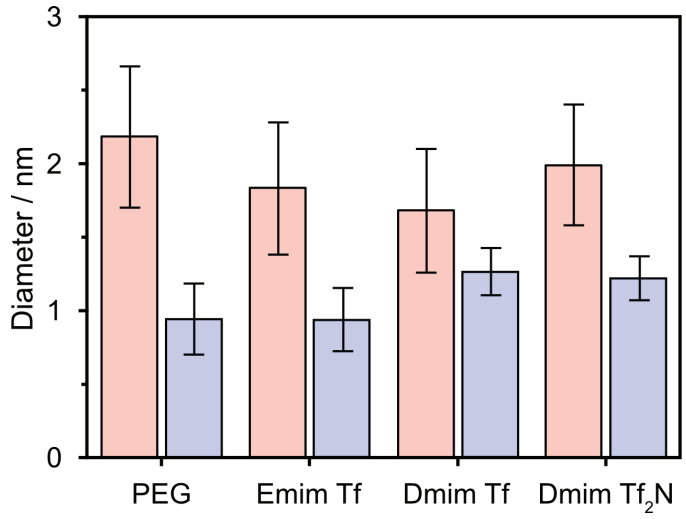

Figure 6.1: Mean platinum nanoparticle sizes, sputtered in four different liquids, evaluated using TEM (red) and SAXS (blue), with error bars indicating standard deviations.

SAXS data, although slightly underestimating the nanoparticle sizes when compared with TEM, confirms the presence of mainly small nanoparticles as shown by the TEM imaging. No clear trends are seen on the nanoparticle size sputtered in different liquids, as all mean diameters are well within one standard deviation of each other.

6.1.2 Substrate temperature

Substrate temperature is well known to affect nanoparticle size in SoL [58], but not much specific data on platinum particles is present in literature. Therefore, in **paper I**, experiments were performed using our unbalanced magnetron to achieve varying degrees of substrate heating by adjusting the sputtering power, while measuring the liquid temperature carefully. Size estimations for platinum nanoparticles sputtered in PEG 600 using 20 W (for 3·300 s), 65 W (for 3·300 s) and 50 W (for 30 s) are shown in figure 6.2. The variations in nanoparticle size, due to sputtering power alteration, is small, evident when comparing the mean size of particles sputtered at 20 W (2.1 nm) and 65 W (2.4 nm). Between particles sputtered at 65 W for 3·300 s and at 50 W for 30 s, the mean sizes differ more, from 2.4 and 1.8 nm, respectively. These

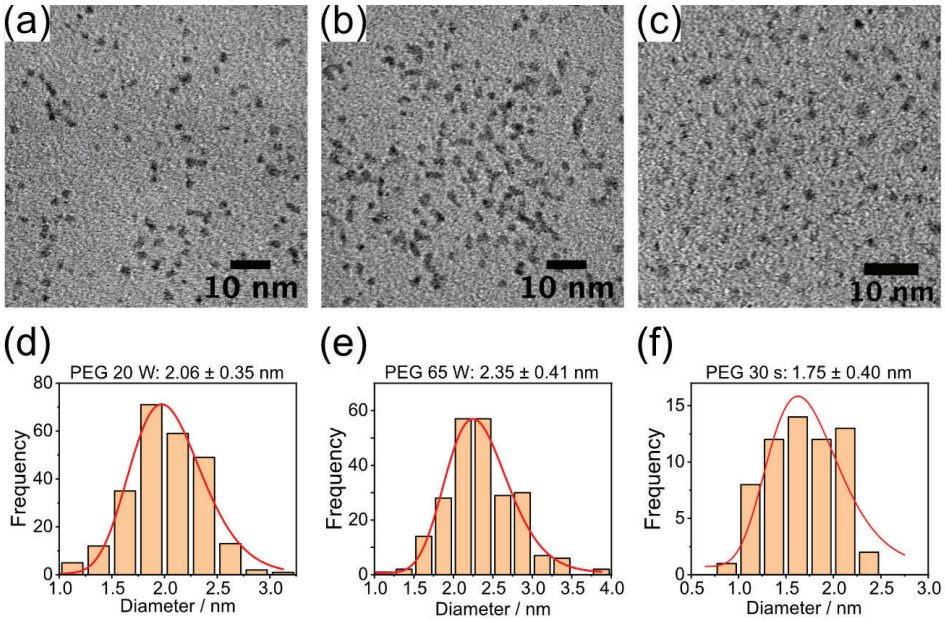

Figure 6.2: TEM micrographs and associated size distribution of platinum nanoparticles sputtered into PEG 600, at 20 W for 3·300 s ((a) and (d)), 65 W for 3·300 s ((b) and (e)), and 50 W for 30 s ((c) and (f)).

results should be viewed in the light of their accompanying temperature data, displayed in figure 6.3. As clearly visible, temperature increases rapidly during the first 100 s of each sputter cycle, after which the increase rate slows down and eventually approaches plateau values closer to the end of each cycle. The heating is considerably faster for the 65 W case, and the maximum temperature reached is just below 200 °C for the high power case, and only 120 °C in the low power case. The temperature development during the 30 s sputtering at 50 W, coincides with the first 30 s of the 65 W cycles, reaching a final temperature of 80 °C at the end of the sputtering experiment.

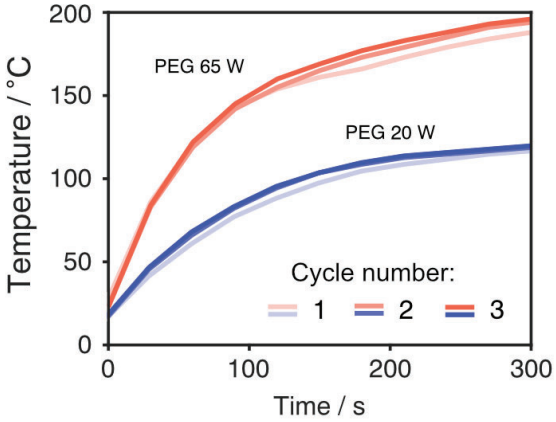

Figure 6.3: Temperature development during sputtering, performed at 20 W (3·300 s), 50 W (30 s) and 65 W (3·300 s), measured using a K-type thermocouple immersed in the liquid.

The effect of substrate temperature on platinum nanoparticle size indicated by these results is small in comparison with what was previously reported for gold [58], a trend similar to what has been observed for gold and platinum grain sizes when sputtered onto flat, solid surfaces [65].

6.1.3 Gas environment

To elucidate the influence of the gas environment on nanoparticle nucleation and growth processes, two approaches was used. First, the influence of the type of sputter gas, on the nanoparticle size was investigated. From the results obtained in **paper I**, it is known that argon sputtering produces small particles with diameters around 2 – 2.5 nm, depending on the liquid temperature, and hence in our case, sputtering power. These are favorable sizes in case of platinum ORR catalysts, but for Pt-RE alloys, increasing the size is crucial to obtain enhanced ORR activity. Therefore, a heavier sputtering gas, krypton, was chosen with the hope that by increasing the impact energy of the sputtering ions, larger clusters of atoms would be ejected, leading to an increase in final nanoparticle size. Figure 6.4a shows a TEM micrograph and size distribution of platinum nanoparticles sputtered into PEG 600 using krypton, at a sputtering power of 50 W. From the size distribution can be observed that the mean size of platinum particles sputtered using krypton is roughly 1.6 nm, which is smaller than particles obtained using argon. This result, while surprising, can be connected back to the previous discussion of sputtering power and substrate temperature: A similar effect was reported by Hatakeyama et al. [66], who used higher sputtering voltages to increase the impact energy of argon ions. They found that smaller gold particles were produced at higher voltages. Concurrently, our results from **paper I** indicate a small size increase for higher sputtering powers, while the sputtering power in turn, increases proportional to the voltage. Hence, the temperature dependence reported in **paper I** may have been underestimated, if the increasing power is in fact counteracting the increase in nanoparticle size. If so, a potential route to increase the size of Pt-RE nanoparticles by magnetron sputtering onto liquids, could be to reduce the sputtering power, while keeping substrate temperatures at an elevated level by external heating.

The second approach regarding influence of the gas environment, was an attempt to estimate the importance of the gas phase in relation to the other groups of parameters. By evaluating the size of nanoclusters sputtered directly onto TEM grids, the aim was to gain an idea of to what extent gas environment affects the nanoparticle nucleation and growth. Figure 6.4b-c shows the medium size of such clusters to be 1.5 nm and 1.4 nm, when sputtered for 0.5 seconds using argon (6.4b) and krypton (6.4c) sputter gas, respectively. These results indicate that clusters arriving at the liquid surface are of similar size to the final nanoparticles, agreeing with a previous report by Deng et al. [67]. This suggests that some growth takes place in the gas phase, and hence, the importance of the gas environment should not be overlooked.

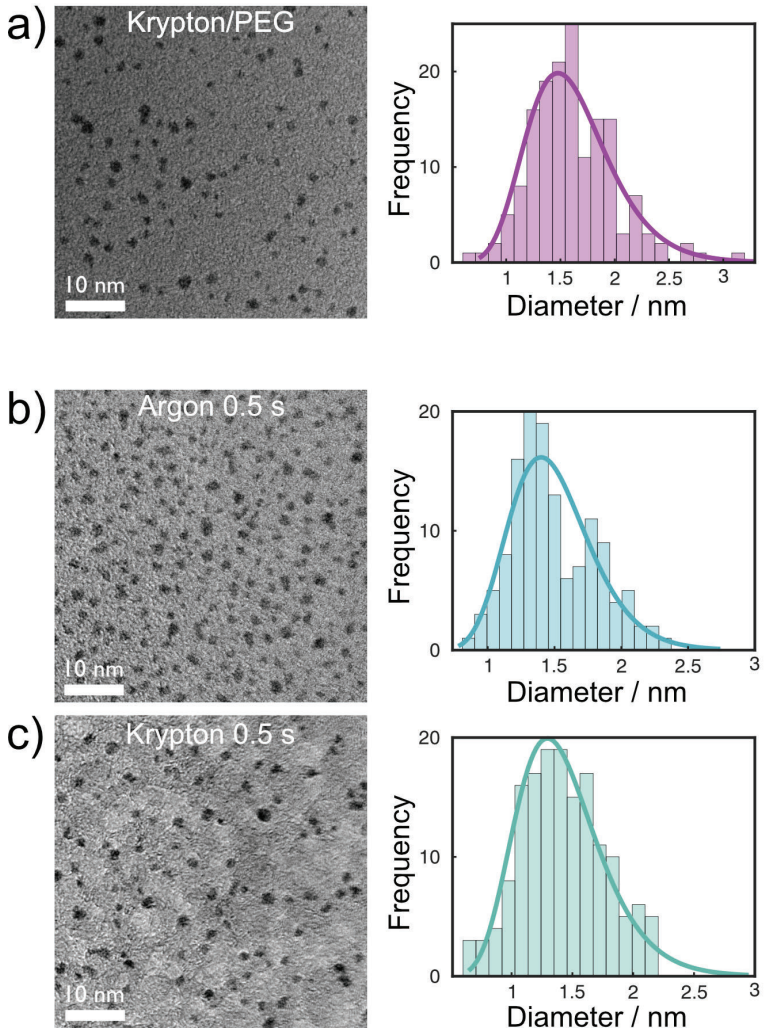

Figure 6.4: TEM micrographs and size distributions of platinum nanoparticles sputtered onto a) PEG 600 using krypton gas, b) TEM grid using argon gas, and c) TEM grid using krypton gas.

6.2 Oxygen reduction evaluated in RDE

The electrochemical evaluation of platinum and Pt_3Y catalysts supported on high surface area carbon support (Vulcan® XC-72) is presented in figure 6.5. Cyclic voltammetry (figure 6.5a) reveals a larger electrochemical surface area in the Pt_3Y sample, which could be a result of either variations in the ink preparation and drop casting, or leaching of oxidized yttrium, from the material. Despite its higher surface area, geometric ORR activity (figure 6.5b), is not increased compared to platinum. As a consequence, after removing the influence of mass transport limitations, the specific kinetic current density of figure 6.5c demonstrates the platinum catalyst as the best performing catalyst. Likely, the small size of primary sputtered particles is not sufficiently large to ensure the presence of metallic yttrium in the particle core, leading to subsequent leaching of yttrium when introduced to the acidic electrolyte of the RDE cell.

The activities showcased in figure 6.5b-c, are high in regards to commercially available platinum catalysts, which typically possess specific activities well

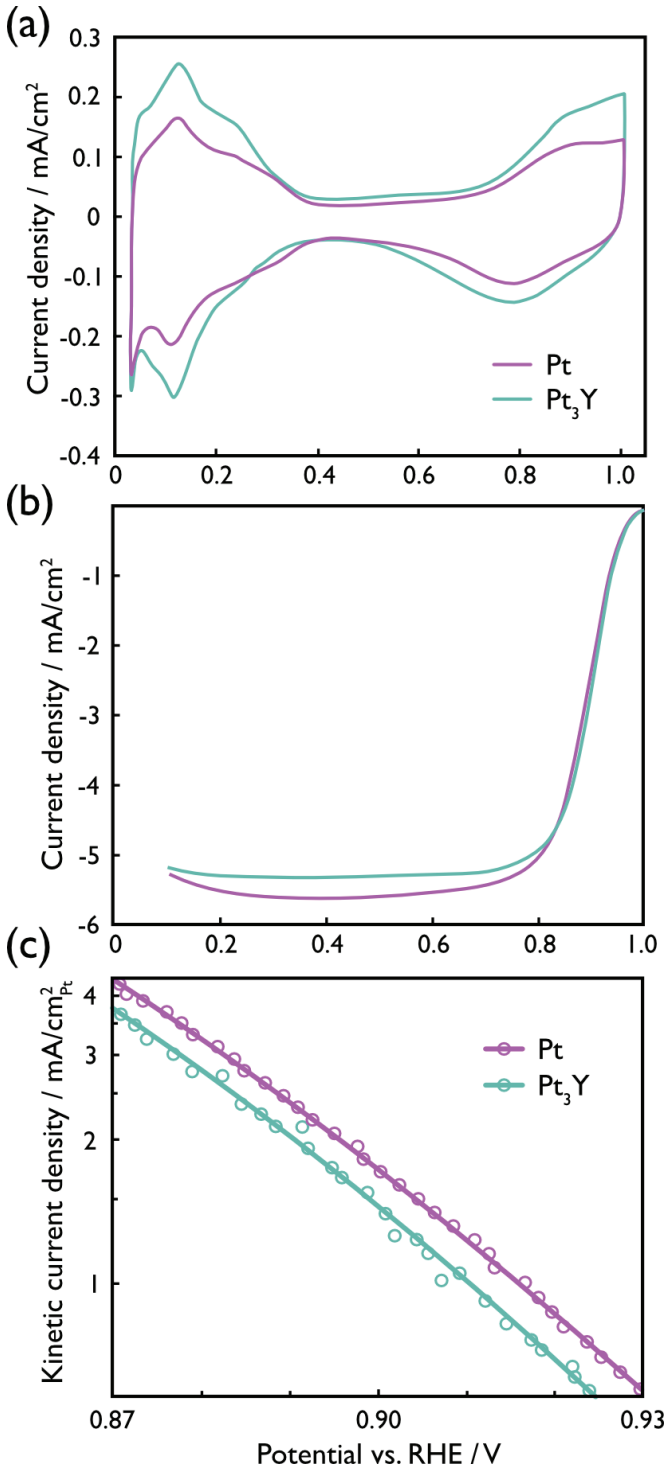

Figure 6.5: Electrochemical characterization of platinum and Pt_3Y carbon supported nanoparticle catalysts. a) Cyclic voltammograms in argon saturated 0.1 M $HClO_4$ electrolyte, b) Geometric ORR activities in oxygen saturated electrolyte, c) Kinetic current densities corrected for mass transport losses. All experiments were recorded at 50 mV/s scan rate.

below 1 mA/cm^2 at 0.9 V. Both platinum and Pt_3Y samples exhibit kinetic current densities of over 1.5 mA/cm^2 at this potential, roughly corresponding to the activity reported for platinum nanoparticles with sizes around 6 – 8 nm [55, 68].

The TEM imaging of the supported platinum nanoparticle catalysts summarized in figure 2 of the **paper II** manuscript, confirms this assumption, as it portrays the existence of two distinct nanoparticle populations in the heat treated, carbon supported catalyst samples. Based on these images, it is evident that the population with the largest particle size (7.1 nm mean diameter), is dominating both in terms of incorporated material, as well as surface area, which is further supported by the electrochemical results. Furthermore, heat treatment of sputtered platinum nanoparticles in the absence of carbon support (**papers I** and **II**), suggest only minor influence on the nanoparticle growth, leaving the presence of carbon particles as the sole explanation for this increase in particle size.

Chapter 7

Conclusions

Platinum-rare earth metal alloy nanoparticles are highly promising as ORR catalysts in PEMFCs, but have so far been notoriously difficult to fabricate without impinging on process scalability. This thesis has introduced a synthesis pathway, based on the sputtering onto liquid (SoL) technique and a simple heat treatment for attachment of nanoparticles onto high surface area carbon. Furthermore, investigations were conducted on the influence of substrate-, magnetron-, and gas environment parameters, on nanoparticle size, to elucidate nanoparticle nucleation and growth mechanisms involved in SoL.

We have identified a small temperature dependence of platinum nanoparticle size, sputtered into PEG 600. The exact interplay between the sputtering power and pure substrate temperature effects, including viscosity, and their effects on the nanoparticle size is yet to be unravelled. However, our results indicate that the positive influence of liquid temperature and viscosity may be counteracted by the use of higher sputtering powers, suggesting that an approach where low sputtering powers are combined with separate substrate heating could be beneficial for larger primary nanoparticle sizes.

There is an influence of the carbon support on catalyst particle size when using our presented heat treatment for nanoparticle-to-support attachment. TEM imaging revealed a dual population of supported nanoparticle sizes which, based on observations included in **papers I** and **II**, can exclusively be explained by further growth of primary catalyst nanoparticles being facilitated on the carbon particle support. The resultant fuel cell catalyst layers, electrochemically evaluated by RDE measurements, exhibit high catalytic performance, with ORR specific activities between 1.5 – 1.8 mA/cm^2 at 0.9 V, and platinum catalysts marginally outperforming those of Pt_3Y. The inferior catalytic activity of Pt_3Y is likely a result of small sputtered primary particles, allowing complete oxidation of yttrium before attachment to carbon support, leading to subsequent leaching during the electrochemical characterization.

The high performance and larger sizes of the platinum-based nanoparticle catalysts obtained herein, is promising for the fabrication of Pt-RE nanoparticles via the SoL synthesis route. To prevent excessive oxidation and leaching of the rare earth alloying agent, further investigations on how to facilitate attachment

of catalyst nanoparticles to carbon support before exposure to oxygen is of high priority. Additionally, optimization of the catalyst-support attachment procedure, to obtain favorable sizes with low levels of particle aggregation, is likely to have great influence on the catalytic activity. Future studies on SoL synthesis of Pt-RE primary particles should address the currently unclear significance of the gas environment, and separate the influence between liquid substrate-, and magnetron related parameters.

In conclusion, this work has demonstrated the viability of using SoL for production of high-performance PEMFC catalyst layers, with potential to be extended to Pt-RE alloy nanoparticles, provided that measures preventing primary particle oxidation is adopted. If successful, such a technological breakthrough could significantly alter the sustainable transport arena, in favor of hydrogen fuel cells.

Acknowledgments

The work in this thesis has been funded by the Swedish Energy Agency (Energimyndigheten).

First and foremost, I would like to thank my supervisor Björn Wickman, and my examiner Henrik Grönbeck, for support and guidance, and for always taking their time to address any questions or issues related to my work.

Then, I would like to express gratitude towards my two co-supervisors, Rosemary Brown and Mathilde Luneau, who supported me and shared their knowledge, at different stages during this work.

I would also like to thank everyone at the Chemical physics division, with a special mention to the past and current members of the Electrochemistry group. You all made this part of the journey a fun and pleasant one.

Finally, to my family and friends who supported me and cheered me on through good and bad, I want to express my greatest appreciation. Without you, none of this would have been possible.

Thank you, everyone!

Bibliography

[1] IPCC. *Synthesis Report of the IPCC Sixth Assessment Report*. 2023. URL: https://www.ipcc.ch/report/ar6/syr/ (cit. on p. 1).

[2] IPCC. *Special Report on Climate Change and Land*. 2019. URL: https://www.ipcc.ch/srccl/ (cit. on p. 1).

[3] IPCC. *Special Report on the Ocean and Cryosphere in a Changing Climate*. 2019. URL: https://www.ipcc.ch/srocc/ (cit. on p. 1).

[4] Naturvårdsverket. *Begränsad Klimatpåverkan*. 2022. URL: https://www.naturvardsverket.se/om-oss/publikationer/7000/begransad-klimatpaverkan/ (cit. on p. 1).

[5] European Commission. *A European Green Deal*. 2020. URL: https://commission.europa.eu/strategy-and-policy/priorities-2019-2024/european-green-deal_en (cit. on p. 1).

[6] IEA. *Net Zero by 2050*. 2021. URL: https://www.iea.org/reports/net-zero-by-2050 (cit. on p. 1).

[7] UNFCCC. *The Paris Agreement*. 2015. URL: https://unfccc.int/process-and-meetings/the-paris-agreement (cit. on p. 1).

[8] UNEP. *Emissions Gap Report 2021*. 2021. URL: https://www.unep.org/resources/emissions-gap-report-2021 (cit. on p. 1).

[9] UNFCCC. *NDC Synthesis Report*. 2022. URL: https://unfccc.int/ndc-synthesis-report-2022#Projected-GHG-Emission-levels (cit. on p. 1).

[10] IEA. *Power Systems in Transition*. 2020. URL: https://www.iea.org/reports/power-systems-in-transition (cit. on p. 1).

[11] European Commission. *EU Hydrogen Strategy*. 2020. URL: https://energy.ec.europa.eu/topics/energy-systems-integration/hydrogen_en#eu-hydrogen-strategy (cit. on p. 2).

[12] Jaime Wisniak. "The History of Catalysis. From the Beginning to Nobel Prizes". In: *Educación Quımica* 21.1 (Jan. 2010), pp. 60–69. DOI: 10.1016/s0187-893x(18)30074-0. URL: https://doi.org/10.1016%2Fs0187-893x%2818%2930074-0 (cit. on p. 3).

[13] Mrs Fulhame. *An Essay on Combustion: With a View to a New Art of Dying and Painting: Wherein the Phlogistic and Antiphlogistic Hypotheses are Proved Erroneous*. author, 1794 (cit. on p. 3).

[14] Athel Cornish-Bawden. *New Beer in an Old Bottle. Eduard Buchner and the Growth of Biochemical Knowledge*. Universitat de València, 1997 (cit. on p. 3).

[15] Jöns Jacob Berzelius. *Årsberättelse om framstegen i fysik och kemi: 1835*. Norstedt, 1835 (cit. on p. 3).

[16] Carl A Busacca et al. "The growing impact of catalysis in the pharmaceutical industry". In: *Advanced Synthesis & Catalysis* 353.11-12 (2011), pp. 1825–1864 (cit. on p. 3).

[17] Ib Chorkendorff and Johannes W Niemantsverdriet. *Concepts of modern catalysis and kinetics*. John Wiley & Sons, 2017 (cit. on p. 3).

[18] M Shelef and R.W McCabe. "Twenty-five years after introduction of automotive catalysts: what next?" In: *Catalysis Today* 62.1 (Sept. 2000), pp. 35–50. DOI: 10.1016/s0920-5861(00)00407-7. URL: https://doi.org/10.1016%2Fs0920-5861%2800%2900407-7 (cit. on p. 3).

[19] P. W. Atkins and L Jones. *Chemical principles*. en. 5th ed. W.H. Freeman, 2010. ISBN: 1-4292-1955-6 (cit. on pp. 3, 7, 9).

[20] R. O'Hayre et al. *Fuel Cell Fundamentals*. 3rd ed. John Wiley & Sons, 2016 (cit. on p. 5).

[21] G Sandstede et al. "Handbook of fuel cells. Fundamentals, technology, applications". In: ed. by W Vielstich, A Lamm and Gasteiger HA. John Wiley & Sons, Ltd Chichester, UK, 2003. Chap. 12. History of low temperature fuel cells, pp. 145–218 (cit. on pp. 7, 13).

[22] F.T. Bacon. "Fuel cells, past, present and future". In: *Electrochimica Acta* 14.7 (July 1969), pp. 569–585. DOI: 10.1016/0013-4686(69)87042-8. URL: https://doi.org/10.1016%2F0013-4686%2869%2987042-8 (cit. on pp. 7, 13).

[23] Carl H. Hamann, Andrew Hamnett and Wolf Vielstich. *Electrochemistry*. 2nd ed. Wiley-VCH, 2007. ISBN: 978-3-527-31069-2 (cit. on pp. 9, 10, 29).

[24] Andrew L Dicks and David AJ Rand. *Fuel cell systems explained*. John Wiley & Sons, 2018 (cit. on pp. 10, 16–18).

[25] Edmund JF Dickinson and Andrew J Wain. "The Butler-Volmer equation in electrochemical theory: Origins, value, and practical application". In: *Journal of Electroanalytical Chemistry* 872 (2020), p. 114145 (cit. on p. 11).

[26] William Robert Grove. "LVI. On a new voltaic combination: To the editors of the Philosophical Magazine and Journal". In: *The London, Edinburgh, and Dublin Philosophical Magazine and Journal of Science* 13.84 (1838), pp. 430–431 (cit. on p. 13).

[27] Eduardo I. Ortiz-Rivera, Angel L. Reyes-Hernandez and Rey A. Febo. "Understanding the history of fuel cells". In: *2007 IEEE Conference on the History of Electric Power*. 2007, pp. 117–122. DOI: 10.1109/HEP.2007.4510259 (cit. on p. 13).

[28] Omar Z Sharaf and Mehmet F Orhan. "An overview of fuel cell technology: Fundamentals and applications". In: *Renewable and sustainable energy reviews* 32 (2014), pp. 810–853 (cit. on pp. 13, 14).

[29] Jung-Ho Wee. "Applications of proton exchange membrane fuel cell systems". In: *Renewable and sustainable energy reviews* 11.8 (2007), pp. 1720–1738 (cit. on p. 14).

[30] Hydrogen and Fuel Cell Technologies Office part of U.S. Department of Energy. *Types of Fuel Cells*. URL: `https://www.energy.gov/eere/fuelcells/types-fuel-cells` (cit. on p. 14).

[31] Hydrogen and Fuel Cell Technologies Office part of U.S. Department of Energy. *Comparison of Fuel Cell Technologies*. URL: `https://www.energy.gov/eere/fuelcells/comparison-fuel-cell-technologies` (cit. on p. 14).

[32] VM Vishnyakov. "Proton exchange membrane fuel cells". In: *Vacuum* 80.10 (2006), pp. 1053–1065 (cit. on p. 15).

[33] Steven J Hamrock and Michael A Yandrasits. "Proton exchange membranes for fuel cell applications". In: *Journal of Macromolecular Science, Part C: Polymer Reviews* 46.3 (2006), pp. 219–244 (cit. on p. 15).

[34] S Jamai Peighambardoust, Soosan Rowshanzamir and Mehdi Amjadi. "Review of the proton exchange membranes for fuel cell applications". In: *International journal of hydrogen energy* 35.17 (2010), pp. 9349–9384 (cit. on p. 15).

[35] L Cindrella et al. "Gas diffusion layer for proton exchange membrane fuel cells—A review". In: *Journal of Power Sources* 194.1 (2009), pp. 146–160 (cit. on p. 16).

[36] Vojislav R Stamenkovic et al. "Improved oxygen reduction activity on Pt3Ni (111) via increased surface site availability". In: *science* 315.5811 (2007), pp. 493–497 (cit. on pp. 19, 20).

[37] Xiaoqing Huang et al. "High-performance transition metal–doped Pt3Ni octahedra for oxygen reduction reaction". In: *Science* 348.6240 (2015), pp. 1230–1234 (cit. on p. 19).

[38] UA Paulus et al. "Oxygen reduction on carbon-supported Pt- Ni and Pt- Co alloy catalysts". In: *The Journal of Physical Chemistry B* 106.16 (2002), pp. 4181–4191 (cit. on p. 19).

[39] V Stamenković et al. "Surface composition effects in electrocatalysis: Kinetics of oxygen reduction on well-defined Pt3Ni and Pt3Co alloy surfaces". In: *The Journal of Physical Chemistry B* 106.46 (2002), pp. 11970–11979 (cit. on p. 19).

[40] Vojislav Stamenkovic et al. "Changing the activity of electrocatalysts for oxygen reduction by tuning the surface electronic structure". In: *Angewandte Chemie International Edition* 45.18 (2006), pp. 2897–2901 (cit. on p. 19).

[41] Patricia Hernandez-Fernandez et al. “Mass-selected nanoparticles of Pt x Y as model catalysts for oxygen electroreduction”. In: *Nature chemistry* 6.8 (2014), pp. 732–738 (cit. on pp. 19, 20).

[42] Ifan EL Stephens, Alexander S Bondarenko and Bech. “Oxygen electroreduction activity and x-ray photoelectron spectroscopy of platinum and early transition metal alloys”. In: *ChemCatChem* 4.3 (2012), pp. 341–349 (cit. on p. 19).

[43] J Greeley et al. “Alloys of platinum and early transition metals as oxygen reduction electrocatalysts”. In: *Nature chemistry* 1.7 (2009), pp. 552–556 (cit. on pp. 19, 20).

[44] Sung Jong Yoo et al. “Pt3Y electrocatalyst for oxygen reduction reaction in proton exchange membrane fuel cells”. In: *International journal of hydrogen energy* 37.12 (2012), pp. 9758–9765 (cit. on p. 19).

[45] Niklas Lindahl et al. “High specific and mass activity for the oxygen reduction reaction for thin film catalysts of sputtered Pt3Y”. In: *Advanced Materials Interfaces* 4.13 (2017), p. 1700311 (cit. on p. 19).

[46] Rosemary Brown et al. “Unraveling the surface chemistry and structure in highly active sputtered Pt3Y catalyst films for the oxygen reduction reaction”. In: *ACS applied materials & interfaces* 12.4 (2019), pp. 4454–4462 (cit. on p. 19).

[47] Niklas Lindahl et al. “Fuel cell measurements with cathode catalysts of sputtered Pt3Y thin films”. In: *ChemSusChem* 11.9 (2018), pp. 1438–1445 (cit. on p. 19).

[48] R Brown et al. “Surface composition of a highly active Pt3Y alloy catalyst for application in low temperature fuel cells”. In: *Fuel Cells* 20.4 (2020), pp. 413–419 (cit. on p. 19).

[49] Amado Velázquez-Palenzuela et al. “The enhanced activity of mass-selected PtxGd nanoparticles for oxygen electroreduction”. In: *Journal of Catalysis* 328 (2015), pp. 297–307 (cit. on pp. 19, 20).

[50] Marıa Escudero-Escribano et al. “Tuning the activity of Pt alloy electrocatalysts by means of the lanthanide contraction”. In: *Science* 352.6281 (2016), pp. 73–76 (cit. on pp. 19, 20).

[51] Kim Degn Jensen et al. “X-ray absorption spectroscopy investigation of platinum–gadolinium thin films with different stoichiometry for the oxygen reduction reaction”. In: *Catalysts* 10.9 (2020), p. 978 (cit. on pp. 19, 20).

[52] Jens Kehlet Nørskov et al. “Origin of the overpotential for oxygen reduction at a fuel-cell cathode”. In: *The Journal of Physical Chemistry B* 108.46 (2004), pp. 17886–17892 (cit. on p. 20).

[53] Shuo Chen et al. “Platinum-alloy cathode catalyst degradation in proton exchange membrane fuel cells: nanometer-scale compositional and morphological changes”. In: *Journal of the Electrochemical Society* 157.1 (2009), A82 (cit. on p. 20).

[54] F Maillard et al. “Durability of Pt3Co/C nanoparticles in a proton-exchange membrane fuel cell: Direct evidence of bulk Co segregation to the surface”. In: *Electrochemistry Communications* 12.9 (2010), pp. 1161–1164 (cit. on p. 20).

[55] Francisco J Perez-Alonso et al. “The effect of size on the oxygen electroreduction activity of mass-selected platinum nanoparticles”. In: *Angewandte Chemie International Edition* 51.19 (2012), pp. 4641–4643 (cit. on pp. 21, 39).

[56] William Robert Grove. “VII. On the electro-chemical polarity of gases”. In: *Philosophical Transactions of the Royal Society of London* 142 (1852), pp. 87–101 (cit. on p. 23).

[57] Gao-xiang Ye et al. “Structural and electrical properties of a metallic rough-thin-film system deposited on liquid substrates”. In: *Physical Review B* 54.20 (Nov. 1996), pp. 14754–14757. DOI: 10.1103/physrevb.54.14754 (cit. on p. 24).

[58] Yoshikiyo Hatakeyama et al. “Synthesis of Gold Nanoparticles in Liquid Polyethylene Glycol by Sputter Deposition and Temperature Effects on their Size and Shape”. In: *The Journal of Physical Chemistry C* 115.8 (Feb. 2011), pp. 3279–3285. DOI: 10.1021/jp110455k. URL: https://doi.org/10.1021%2Fjp110455k (cit. on pp. 25, 34, 36).

[59] Jaydeep Sarkar. “Sputtering and Thin Film Deposition”. In: *Sputtering Materials for VLSI and Thin Film Devices*. Elsevier, 2014, pp. 93–170. DOI: 10.1016/b978-0-8155-1593-7.00002-3. URL: https://doi.org/10.1016%2Fb978-0-8155-1593-7.00002-3 (cit. on p. 25).

[60] Peter W. Hawkes and John C. H. Spence, eds. *Springer Handbook of Microscopy*. Springer Cham, 2019. ISBN: 978-3-030-00069-1 (cit. on pp. 26, 27).

[61] L. A. Feigin and D. I. Svergun. *Structure Analysis by Small-Angle X-Ray and Neutron Scattering*. en. Springer, 2013. ISBN: 978-1-4757-6624-0 (cit. on p. 27).

[62] Paul van der Heide. *X-Ray Photoelectron Spectroscopy*. en. Wiley & Sons, Incorporated, John, 2011. ISBN: 9781118162927 (cit. on p. 27).

[63] S Trasatti and OA Petrii. “Real surface area measurements in electrochemistry”. In: *Pure and applied chemistry* 63.5 (1991), pp. 711–734 (cit. on p. 31).

[64] T Biegler, DAJ Rand and R Woods. “Limiting oxygen coverage on platinized platinum; relevance to determination of real platinum area by hydrogen adsorption”. In: *Journal of Electroanalytical Chemistry and Interfacial Electrochemistry* 29.2 (1971), pp. 269–277 (cit. on p. 31).

[65] Rod Heu et al. “Target material selection for sputter coating of SEM samples”. In: *Microscopy Today* 27.4 (2019), pp. 32–36 (cit. on p. 36).

[66] Yoshikiyo Hatakeyama, Kei Onishi and Keiko Nishikawa. “Effects of sputtering conditions on formation of gold nanoparticles in sputter deposition technique”. In: *RSC advances* 1.9 (2011), pp. 1815–1821 (cit. on p. 36).

[67] Lianlian Deng, Mai Thanh Nguyen and Tetsu Yonezawa. “Sub-2 nm single-crystal Pt nanoparticles via sputtering onto a liquid polymer”. In: *Langmuir* 34.8 (2018), pp. 2876–2881 (cit. on p. 36).

[68] Chao Wei et al. “Recommended practices and benchmark activity for hydrogen and oxygen electrocatalysis in water splitting and fuel cells”. In: *Advanced Materials* 31.31 (2019), p. 1806296 (cit. on p. 39).